Air quality intervention altered the emission sources and chemical composition of size-segregated urban inhalable PM leading to mitigated cytotoxic responses in *in vitro* co-culture model

or

Air quality intervention during Nanjing Youth Olympic Games affected PM sources, chemical composition, and toxicological responses in *in vitro* co-culture model

Teemu J. Rönkkö[a], Maija-Riitta Hirvonen[a], Mikko S. Happo[a], Ari Leskinen[b,c], Hanna Koponen[a], Santtu Mikkonen[c], Stefanie Bauer[d], Tuukka Ihantola[a], Henri Hakkarainen[a], Mirella Miettinen[a], Jürgen Orasche[d,e], Cheng Gu[f], Qin'geng Wang[f], Jorma Jokiniemi[a], Mika Komppula[b], Olli Sippula[a], Pasi I. Jalava[a]

a University of Eastern Finland, Department of Environmental and Biological Sciences, Yliopistonranta 1, P.O. Box 1627, FI-70211 Kuopio, Finland
b Finnish Meteorological Institute, Yliopistonranta 1, P.O. Box 1627, FI-70211 Kuopio, Finland
c University of Eastern Finland, Department of Applied Physics, Yliopistonranta 1, P.O. Box 1627, FI-70211 Kuopio, Finland
d German Research Center for Environmental Health, Helmholtz Zentrum München, Munich, Germany
e Joint Mass Spectrometry Center, Cooperation Group Comprehensive Molecular Analytics, German Research Center for Environmental Health, Helmholtz Zentrum München, Munich, Germany
f Nanjing University, School of the Environment, Branch 24 Mailbox of Nanjing University Xianlin Campus, No. 163 Xianlin Avenue, Qixia District, 210023 Nanjing, China

Abstract

Ambient Particulate matter (PM) is among the leading environmental health risks globally. Current air quality regulations assume that PM toxicity is only affected by airborne mass concentration. However, recent evidence indicates that PM from different sources with distinct chemical compositions have varied toxic potencies. Several factors, such as emission control measures, contribute to the variability in air quality, thus their influences are under rigorous investigation. Yet, the connections between induced changes in PM composition and toxicity are insufficiently elucidated. We exposed co-cultures of A549 and THP-1 cells to size-segregated inhalable PM collected in Nanjing, China before, during, and after an air quality intervention for the 2014 Youth Olympic Games. The co-culture models the alveolar epithelium with the associated macrophages. Additionally, we investigated the PM composition, local meteorological parameters, and aerosol trajectories. This paper presents how sampling campaigns and emission restrictions, location, time of day, and chemical composition influenced the PM-induced cytotoxicity and

oxidative stress in the co-culture model, along with how the emission control period changed the composition and emission source contributions of PM.

We observed that emission control measures drastically reduced PM_{10} mass concentrations by over 50 % and changed the emission source contributions and PM composition. The role of traffic and fuel combustion emissions were magnified during the emission control period. Our analyses revealed that the PM samples demonstrated differential cytotoxic potencies at equal mass concentrations between sampling campaigns, locations, and time of day, influenced by variations in the predominant emission sources and PM composition. Coal combustion and industrial emissions were the most important sources affecting the toxicological responses and displayed the least variation in emission contributions between the sampling campaigns. In conclusion, emission control mitigated cytotoxicity and oxidative stress for particles larger than 2 µm, but there was inadequate evidence to determine if it was the key factor reducing the harmful effects of $PM_{0.2}$.

1. Introduction

Rapid industrialization and economic growth during the past three decades have generated sharply increased air pollution levels and severe air quality problems in China. A nationwide total emission control (TEC) policy was introduced in 1996, yet the air pollution issue aggravated rapidly through the 2000s. The nationwide TEC policy has several important shortcomings including too broad scale for the employed method, removal of several important pollutants from the list of targeted pollutants over the years, and inadequate scientific grounds for determining emission quotas and reduction targets as well as assessing emission reductions (Hu et al. 2018). A more stringent direction in emission controls commenced in 2013 when the central government issued a clean air action plan, followed by revision of the environmental protection law in 2014. However, the gravity of the worsening air quality problem was highlighted in December 2015 with over 40 Chinese cities engulfed in heavy smog and $PM_{2.5}$ levels reaching above 300 $\mu g/m^3$. Several periods of extremely low air quality followed during 2016 and 2017. The emission control policies enacted in 2013-2014 have resulted in a 39.5 % reduction of ambient $PM_{2.5}$ level and a 12.6 % reduction of $PM_{2.5}$ attributable premature deaths in mainland China from 2013 to 2017 (Zou et al. 2019). Yet, PM still poses an enormous health problem requiring further focus, not only in the priority air pollution control areas, such as the whole of coastal Eastern China including the Yangtze River Delta, but in non-priority areas as well.

Harsh temporary emission control measures have often been imposed during important national and international events, such as the 2008 Beijing Olympics; these measures typically include shutting down polluting factories and restrictions on traffic and construction projects. However, smog and high PM levels have usually returned quickly after the end of these short-term local air quality interventions. Thus, finding impactful air pollution reduction strategies is a priority for the developing economies struggling with air pollution.

Ambient particulate matter is among the greatest risk factors for human health worldwide. Chronic exposure to PM is associated with increased morbidity and mortality due to a diverse set of detrimental human health outcomes, including cardiovascular diseases, stroke, Alzheimer's, and asthma (Cohen et al. 2017, Forouzanfar et al. 2015, Mazidi & Speakman 2017, Pearson et al. 2010, Portnov et al. 2012). According to the Global Burden of Disease 2016 study, ambient PM is the third leading risk factor attributable to 1.1 million deaths in China, mainly due to cardiovascular diseases (Gakidou et al. 2017). Another study estimated the premature mortality burden of $PM_{2.5}$ in China as

high as 1.5 million deaths in 2015, and 1.7 million deaths after a 10-year lag period (Song et al. 2017). Recent estimates of mortality caused by ambient $PM_{2.5}$, based on hazard ratios on a global range of $PM_{2.5}$ concentrations, were even higher than those calculated previously from Western cohort studies where $PM_{2.5}$ concentrations were rather low compared to those seen in, for example, China (Burnett et al. 2018). Many of these estimates and risk assessment of PM in general is based on the assumption that PM toxicity is directly linked to its airborne mass concentration alone. However, several studies have illustrated that the PM chemical composition, and by extension emission sources, heavily influence the toxicological responses (Abbas et al. 2018, Ghio et al. 2014, Jin et al. 2019, Park et al. 2018, Velali et al. 2018), yet causal correlations between adverse health effects and individual PM components are yet to be found.

An example of temporary efforts to reduce air pollution occurred in Nanjing, the capital of Jiangsu province in the Eastern China, in preparation for the Youth Olympic Games during August 16-28, 2014. Nanjing is a heavily industrialized megacity of over 8 million inhabitants located in the western part of the densely populated and highly developed Yangtze River Delta region. Emissions from coal-powered industries, metallurgic and chemical industries, vehicular transportation, and construction, contribute heavily to the local urban aerosol concentration and composition (Qi et al. 2016, Wang et al. 2016, Yuan et al. 2017). Furthermore, long-range transport of aerosols from Yangtze River Delta and Northern China can bring pollutants, such as biomass and coal combustion emissions, from distant sources into the Nanjing atmosphere. Similar to many large Chinese cities, Nanjing has experienced several recent poor air quality events. The Youth Olympic Games prompted local efforts to restrict air pollution and PM levels in Nanjing and provided a unique opportunity to study how this air quality intervention affected the chemical composition of PM in Nanjing and the resulting toxicological responses.

In this study, we investigated the effects of weather conditions, composition of PM, and the dominant emission sources on cytotoxic and oxidative stress responses caused by PM exposure in a co-culture model of human alveolar epithelial cells and macrophages. To this end, we collected size-segregated PM samples of four size fractions ($PM_{10-2.5}$, $PM_{2.5-1.0}$, $PM_{1.0-0.2}$, and $PM_{0.2}$) separately during day- and nighttime in May-June (pre-intervention campaign), August (intervention), and October-November (post-intervention) 2014 in Nanjing. We performed the PM sampling at an urban background location for all campaigns; additionally, during the intervention and post-intervention campaigns, PM samples were also collected in downtown Nanjing. These two sampling locations allowed us to compare the effects of the air quality intervention in two distinct urban locations with different emission profiles, as well as to assess the local spatial variations in PM composition and cytotoxicity.

This paper describes the results of meteorological, chemical, and toxicological analyses and discusses how the air quality intervention influenced the PM composition and the concomitant cytotoxicity effects and oxidative stress.

2. Materials and methods

2.1. Sample collection and preparation

We conducted three sampling campaigns in Nanjing, China during May-June (28.5.-14.6., pre-intervention), August (15.8.-27.8., intervention), and October-November (22.10.-5.11., post-intervention) 2014. During all the campaigns, the sample collection site was located at the Nanjing

University Xianlin Campus, described in detail in our previous paper (Rönkkö et al. 2018). Additionally, during the August and October-November campaigns a second sample collection site in downtown Nanjing at the Nanjing University Gulou Campus (koordinaatit) was included. Samples were collected separately at day and night. The three sampling campaigns represent different air pollution situations before, during, and after an air quality intervention/emission reduction measures, which were in effect to reduce air quality problems during the Nanjing Youth Olympic Games in August 2014.

We collected the PM samples using a modified Harvard High Volume Cascade Impactor (HVCI) (Jalava et al. 2006, Sillanpää et al. 2003), as described in detail by (Jalava et al. 2015). We segregated the PM into four size fractions according to their aerodynamic diameter: $PM_{10\text{-}2.5}$ (10-2.5 µm), $PM_{2.5\text{-}1.0}$ (2.5-1.0 µm), $PM_{1.0\text{-}0.2}$ (1.0-0.2 µm) and $PM_{0.2}$ (<0.2 µm) particles. We collected $PM_{10\text{-}2.5}$, $PM_{2.5\text{-}1.0}$ and $PM_{1.0\text{-}0.2}$ samples on polyurethane foam (PUF) substrates, and $PM_{0.2}$ on polytetrafluoroethylene (PTFE, Fluoropore 3.0 µm FSLW) backup filters. Three field blank filter sets for each campaign, sampling location, and size fraction were prepared and used as negative controls in the toxicological studies. The procedure for the preparation of the collected PM samples for chemical and toxicological analyses has been described previously by (Jalava et al. 2015, Tapanainen et al. 2012).

2.2.PM composition

Inorganic elements, anions, PAHs and OPAHs were analyzed as described previously in (Rönkkö et al. 2018). The chemical analyses were performed on dried, methanol-extracted PM samples, similarly to the toxicological analyses. Briefly, several metals and other elements were analyzed by inductively coupled plasma mass spectrometer (ICP-MS) after elution with HNO_3 and HF according to standard EN ISO 17294-2. Anions were analyzed by ion chromatography according to standard EN ISO 10304-1/2 after elution with NaOH and Na_2CO_3. Most unsubstituted and alkylated PAHs were analyzed using gas chromatography mass spectrometry (GCMS) with selected ion monitoring (SIM) mode as described in detail by (Sippula et al. 2013). Selected PAHs as well as oxygenated and sulfurated PAHs were analyzed by thermal desorption GC-MS after extraction with dichloromethane as described in (Rönkkö et al. 2018). The sum of known genotoxic PAH compounds was calculated according to (World Health Organization, International Programme on Chemical Safety 1998). Organic (OC) and elemental carbon (EC) contents of the PM samples were analyzed with a thermal-optical carbon analyzer (Lab OC-EC Aerosol Analyzer, Sunset Laboratory, USA) following the NIOSH 5040 (NIOSH Manual of Analytical Methods, 2003) analysis protocol. For each analysis, 250 µl of sample in methanol suspension were injected on a piece of a quartz fiber filter (TissuquartzTM Filters, Pall Corporation, USA) and the analysis was conducted as described previously by (Kasurinen et al. 2017).

2.3.Meteorological parameters and air mass trajectories

Methods concerning meteorological parameters, air quality, and air mass origins were identical as reported previously in (Miettinen et al. 2018, Rönkkö et al. 2018). Briefly, ambient temperature (°C), pressure (mbar), relative humidity (%), wind speed (m s^{-1}) and direction (°), and rain accumulation (mm) were measured with a Vaisala Model WXT520 weather station. The weather station was located approx. 2 m above the container roof, minimizing disturbances by the nearby objects. A radiation and rain shield was used for the humidity and temperature sensors. The meteorological data was acquired with a time resolution of 1 min.

We calculated backward air mass trajectories using the PC-based HYSPLIT model (Rolph et al. 2017, Stein et al. 2015) for the preceding 120 hours with a 1-hour time resolution. From the trajectory calculations, we obtained the air mass coordinates and height above ground level at each hour. Rainfall, terrain height, and the mixing depth of the model outputs were also applied in the analysis.

The trajectories were assigned to five sectors according to their coordinates: 1) "Yellow Sea" (0–90 degrees), 2) "East China Sea + Shanghai" (90–135 degrees), 3) "Southern China" (135–225 degrees), 4) "Southwestern China" (225–270 degrees), and 5) "Northwestern China" (270–360 degrees). For these sectors, we assumed different types of aerosols. Aerosols from sectors 1–3 were a mixture of marine and continental origin, including parts of the Northern China, the Korean peninsula, and Japan (sector 1), marine air masses influenced by the highly polluted Yangtze River Delta region including the megacity of Shanghai (Sector 2), and a mixture of marine aerosol and the Southern megacities such as the Guangzhou–Shenzen–Hong Kong region (Sector 3). The air masses from the sectors 4 and 5 were expected to be completely of continental origin, including Southwestern China with less wintertime heating of houses (Sector 4) and Northwestern China where houses are heated during the winter (Sector 5).

2.4.Cell culture, PM exposure, and toxicological analyses

Cells were cultured and seeded in the co-culture 12-well plates for exposure as described in (Kasurinen et al. 2018). Briefly, A549 human adenocarcinomic alveolar epithelial cells were purchased from ATCC (ATCC® CCL-185). THP-1 human monocyte cells (DSMZ ACC 16) were purchased from the German Collection of Micro-organisms and Cell Cultures (DSMZ, Germany). Both cell lines were maintained in Dulbecco's Modified Eagle Medium (DMEM, Sigma-Aldrich, USA) supplemented with 10 % fetal bovine serum (FBS), 2mM L-glutamine (L-glut), and 100 U/ml penicillin/streptomycin (pen/strep) (all Sigma-Aldrich, USA).

For the exposure experiments, A549 cells were seeded in the 12-well plates at a density of 120.000/ml/well, followed by a 4-hour attachment period in the incubator before seeding 24.000/ml/well differentiated and washed THP-1 cells on top. THP-1 cells were differentiated into macrophage-like cells with phorbol 12-myristate 13-acetate (PMA) prior to seeding them onto the 12-well plates. $15x10^6$ to $20x10^6$ cells from a maintenance flask were centrifuged and resuspended in 10 ml culture medium containing 0.5 µg/ml PMA. The cell suspension was incubated for 90 minutes in a new culture flask at 37 °C, 5 % CO_2 in a humidified incubator. This was followed by aspiration of the cell suspension and rinsing of the attached cells by Dulbecco's phosphate buffered saline (PBS), and two subsequent washes with PBS. The co-cultured cells were incubated for 40 hours at 37 °C, 5 % CO_2 before the exposure to the PM samples. Cell density at the end of the 24-hour exposure period was approx. 400.000-600.000 cells/ml (approx. 105.000-160.000 cells/cm^2).

One hour before exposure of the cells with the PM samples, the culture medium was replaced and the PM samples resuspended into 10 % dimethyl sulfoxide (DMSO) in embryo transfer water (W1503, Sigma-Aldrich) and sonicated for 30 minutes. Three doses (50, 100, and 200 µg/ml, corresponding to 13.2, 26.3, and 52.6 µg/cm^2) of the PM samples were administered onto the cells, and the cell plates were incubated for 24 h at 37 °C, 5 % in a humidified incubator. Method-specific positive exposure agents were included in the exposure setup: etoposide (1.5 µM) for cell cycle analysis, lipopolysaccharide (LPS, 0.02 µg/ml) for inflammation, methyl methane sulfonate (MMS, 0.0015%) for genotoxicity, as well as solvent (DMSO, 0.4 %) and filter blank controls (corresponding

to the 200 µg/ml PM dose). Each independent exposure experiment was performed four times yielding n = 4 for all endpoint analyses unless stated otherwise.

Oxidative stress

Intracellular oxidative burden: For the analysis of intracellular oxidative stress by 2',7'-dichlorofluorescein diacetate (H_2DCF-DA), a 200 µl aliquot of cell suspension was centrifuged and supernatant was removed, and the cells resuspended in 220 µl PBS to remove FBS, which interferes with the 2',7'-dichlorofluorescein (DCF) fluorescence measurement. 100 µl duplicate aliquots of the cell suspension were applied on a 96-well plate, followed by addition of 8 µl of H_2DCF-DA (0.5 µM in DMSO) in the wells. DCF fluorescence was measured immediately and at 30 and 60 minutes after the addition of H_2DCF-DA (excitation 485 nm, emission 530 nm, VICTOR3™ Multilabel Counter model 1420-051, PerkinElmer, USA). Measured fluorescence unit values were plotted against time, and the area under the curve (AUC) was calculated from the average fluorescence of the duplicates for each sample. AUC values were normalized to unexposed controls by dividing the AUC for exposed cells by the AUC of unexposed control cells.

Cytotoxicity

Cell membrane integrity: cell membrane permeability was measured by propidium iodide (PI) from the same 96-well plate as oxidative stress by H_2DCF-DA. After the 60 min DCF fluorescence measurement, 7.2 µl of PI (0.5 mg/ml in PBS) was added into the wells, followed by a short shaking of the plate on a plate-shaker, and a 20-minute incubation at 37 °C, 5 % in a humidified incubator. Baseline fluorescence (F1) was read by multiplate reader (excitation 540 nm, emission 610 nm), after which 20 µl of 10 % Triton-X100 (v/v, in ddH_2O) was added into each well. The plate was incubated at RT, under gentle shaking, in the dark on a plate-shaker. The final PI fluorescence (F2) was read with the same wavelengths as above. Proportion of membrane-compromised and thus unviable cells was calculated by the following formula: percentage PI-positive cells = F1/F2*100.

Cellular metabolic activity: CMA was analyzed from two 100 µl duplicate aliquots from each sample by adding 25 µl of 3-(4,5-dimethylthiazol-2-yl)-2,5-diphenyltetrazolium bromide (MTT, 5 mg/mL in PBS) in each sample well on a 96-well plate, followed by 2-hour incubation at 37 °C, 5 % CO_2. This was followed by a 100 µl addition of sodium dodecyl sulfate (SDS) lysis buffer (0.2 g/ml SDS in 50 % (v/v) ddH20, 50 % (v/v) dimethylformamide (DMF)). The plate was incubated at 37 °C, 5 % CO_2 overnight before reading absorbance at 570 nm in a multiplate reader (VICTOR3™ Multilabel Counter model 1420-051, PerkinElmer, USA). The results were normalized by dividing the absorbance produced by exposed cells by that of unexposed control cells.

Cellular viability: For the analysis of cellular viability by 4',6'-diamidino-2-phenylindole (DAPI) and AO using NucleoCounter NC-3000 fluorescence image analyzer, a 19 µl aliquot of each sample was transferred to an Eppendorf tube followed by the addition of 1 µl of staining Solution 13 (100 µg/ml DAPI, 30 µg/ml AO). Cell suspension was mixed rigorously before applying 11 µl onto NucleoCounter A8-slides and analyzing the vitality with the appropriate protocol provided by the manufacturer.

2.5.Statistical analyses

Differences in cellular metabolic activity due to sampling campaigns, location, and time of day, with exposure as the covariate, were analyzed with a factorial multiple regression model by SPSS's General Linear Model (GLM) separately for each PM size fraction. Linearity of dose-response and normal distribution of the dependent variable were assessed by scatter plots. Homogeneity of

regression slopes was inspected with GLM by assessing the interaction effects of independent variables and exposure dose; interaction term with $p < 0.05$ indicated significantly differing regression slopes depending on the value of that independent variable. Significant interaction terms between independent variable and exposure dose, and between two independent variables were retained in the model whereas non-significant interaction terms were left out of the factorial model one by one in descending order of interaction level and observed p-values. Levene's test for equality of error variance as well as scatter plots of the residuals were used to inspect the normal distribution of the residuals. Sidak's adjustment of confidence intervals was employed for multiple post-hoc comparisons.

Principal component analysis (PCA) was performed on the chemical component dataset of all PM size fractions and sampling campaigns described in this study to determine the principal components (PCs) explaining variations in the chemical profile of the collected PM samples. The authors are aware that pooling all the PM size fractions this way slightly complicates the interpretation of the results linking chemical composition to toxicological effects, since the resulting PCs make no distinction between PM size fractions even though they differ in chemical composition and toxicological responses. This is a limitation dictated by the size of the current dataset. Technical details……The PCs were assigned to scientifically plausible emission sources depending on the loading values of the identified chemical components.

Some kind of mixed model analysis was performed to assess how the chemical PCs and select individual chemical components (mainly toxic metals) contributed to the observed toxicological responses. Technical details… PM size fraction and sampling location were assigned as random effects due to the non-independence of chemical composition within each level of these factors.

Comparison of the rank of effect size in the model for each PC was conducted by removing each PC from the model, in turn, one at a time, and comparing the changes of Schwarz's Bayesian Criterion (BIC) value. Larger changes in BIC indicate larger explanatory power of the removed PC on the dependent variable, i.e. toxicological endpoint.

Statistical analyses were performed using IBM SPSS version 25 and R software (versio).

3. Results and discussion

In this study, we report that the air quality intervention during the Nanjing Youth Olympic Games 2014 altered the composition of urban inhalable PM, which resulted in mitigated cytotoxicity and oxidative stress for particle fractions larger than 200 nm in diameter. $PM_{0.2}$, however, displayed no evidence that the air quality intervention alone was responsible for the reduced cytotoxic or oxidative responses, suggesting the importance of seasonal variation in PM composition for toxicological effects. We studied the toxicological effects using a co-culture model of human alveolar surface utilizing cell lines modelling the alveolar epithelial cells (A549) and alveolar macrophage-like cells (THP-1). Furthermore, we describe the chemical composition of the size-segregated PM and discuss the derived principal emission sources as well as the meteorological parameters and atmospheric processes that influence the chemical composition. Finally, we discuss how the air quality intervention and the PM composition affected the observed toxicological responses.

As summarized previously by (Miettinen et al. 2018), the emission control measures in Nanjing for the 2014 Youth Olympic Games began in June with the shutting down of coal-powered industries, a process that was finished by July 15 (Ding et al. 2015). Restriction on construction works

commenced on July 15 when one third of construction sites were temporarily shut down; a further 2000 construction sites were closed during August 1-15, and finally all construction was stopped between August 16-31. Additionally, high emission vehicles were banned, and the manufacturing output of heavy industries was required to be cut by 20 % during August. Furthermore, during August 1-31, Nanjing and 22 surrounding cities collaborated to improve the regional air quality by using high quality coal in the industrial plants, and reducing power generation by 15 % (Zhao et al. 2017, Zhou et al. 2017).

Table 1: Summary of sampling durations, local weather conditions in Nanjing, and air mass trajectory analysis. Averaged results.

	Pre-intervention		Intervention		Post-intervention	
	Day	Night	Day	Night	Day	Night
Sampling duration (h)	9.2	13.4	8.4	13.6	8.5	14.0
T (°C)	28.2 ± 3.8	24.9 ± 3.2	26.0 ± 2.7	24.1 ± 2.1	19.2 ± 3.6	15.9 ± 3.2
RH (%)	47.5 ± 15.5	60.0 ± 15.0	69.1 ± 10.6	78.9 ± 7.2	56.0 ± 20.0	69.5 ± 13.8
p (mbar)	1001.0 ± 1.9	1001.0 ± 1.8	1005.8 ± 2.8	1005.6 ± 2.3	1015.7 ± 3.4	1015.9 ± 3.1
Wind direction (°)	50.7 ± 35.9	93.5 ± 40.3	63.3 ± 34.4	91.0 ± 41.0	146.2 ± 39.6	55.4 ± 44.5
Wind speed (m/s)	2.7 ± 1.6	1.8 ± 1.2	2.0 ± 1.2	1.4 ± 1.0	2.3 ± 1.4	1.7 ± 1.3
Rain sum (mm)	44.1	5.2	20.7	12.8	9.0	5.5
Calm (% of time)	11.4	35.3	23.1	46.0	20.2	40.1
Main sectors	1, 2	1, 2	1, 2	1, 2	1, 5	1, 5
Sector1 (%)	44.1	50.6	57.1	58.7	39.3	39.4
Sector2 (%)	27.9	21.4	15.6	18.9	8.7	10.2
Sector3 (%)	18.0	13.0	11.4	7.0	13.1	12.6
Sector4 (%)	3.0	4.2	1.6	3.7	0.5	1.1
Sector5 (%)	7.1	10.7	14.3	11.7	38.4	36.7
Air mass height above sea level (m)	265.6	532.5	310.2	308.4	1293.8	1203.2
Height above ground level (m)	224.5	452.3	286.1	280.1	1022.5	908.8
Mixing depth at measurement site (m)	1148.7	533.6	564.8	214.2	627.8	275.4
In mixing layer (%)	69.5	70.9	75.7	76.1	59.0	59.2
Above mixing layer (%)	30.5	29.1	24.3	23.9	41.0	40.8
Time after last rainfall (h)	74.9	74.2	19.2	15.1	76.2	74.5
Over sea (%)	53.3	46.9	48.7	48.0	19.9	19.3
Time after last sea touch (h)	37.0	37.5	38.8	41.4	46.7	49.6

3.1. Meteorological conditions and air mass trajectories

Table 1 presents a summary of the weather conditions and air mass trajectory analysis for the three sampling campaigns, separately for day and night. The data for the individual sample collections are available in (Supplementary material). The temperatures during the campaigns were typical for the seasons. The average temperature difference between day and night was 3.3 °C during the pre-intervention and post-intervention campaigns. During the intervention campaign, the nights were relatively warmer and more humid than during the other campaigns. The average relative humidity during the nights in the pre-intervention campaign was 78.9 %. The atmospheric pressure was highest during the post-intervention campaign, indicating a dominant high pressure area with less rainfall. As expected, wind speeds were higher during daytime compared to night. Rainy periods occurred mainly in the daytime as well. Wind directions were similar for the pre-intervention and intervention campaigns with daytime northeasterly and nighttime easterly winds, whereas for the post-intervention, the daytime winds were shifted to mainly southeasterly winds and to northeasterly for nighttime.

The dominating sector for the air masses was Sector 1 during all campaigns, both during the day and nighttime. During the pre-intervention campaign, the secondary sector was Sector 2, and the air masses were mainly of marine origin. During the intervention, the air masses were more evenly distributed between the other sectors than Sector 1. For the post-intervention campaign, the

secondary sector was Sector 5, resulting in a mixture of marine and continental air masses (Table 1 and Figure 1). The air masses had spent the last 120 hours mainly in the mixing layer, and there were no remarkable differences between the daytime and nighttime. The percentage in the mixing layer was lowest, 59 %, for the post-intervention campaign, where the average height above ground level was the highest. This may reduce the influence of distant emission sources during the post-intervention campaign and emphasize the role of local emission sources in and around Nanjing.

The time after last rainfall was the lowest for the intervention campaign. This means that the air mass may be cleaner than during the other campaigns due to particle wet deposition - or that it is mainly influenced by emission sources nearer the sampling sites. Additionally, the trajectory pattern during campaign 5 was more concentrated in the vicinity of Nanjing, further emphasizing the effects of local and nearby emission sources.

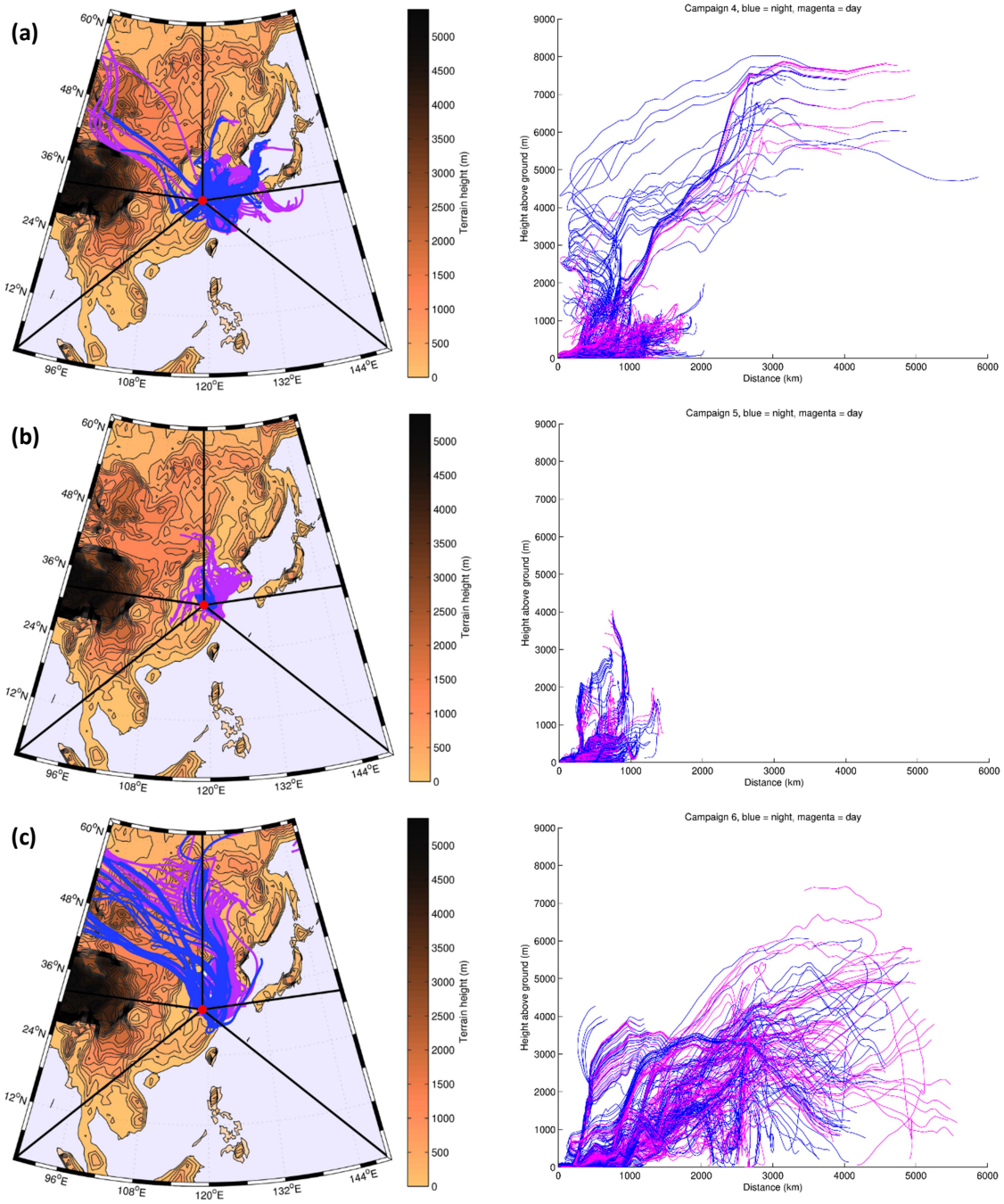

Figure 1: Air mass trajectories during the sampling campaigns: (a) pre-intervention, (b) intervention, (c) post-intervention. On the left pane, magenta trajectories depict air masses with no rainfall in the last 120 h, blue trajectories depict air masses with rainfall during this time. On the right pane, magenta depicts the height of daytime air mass trajectories and blue depicts this for nighttime air masses.

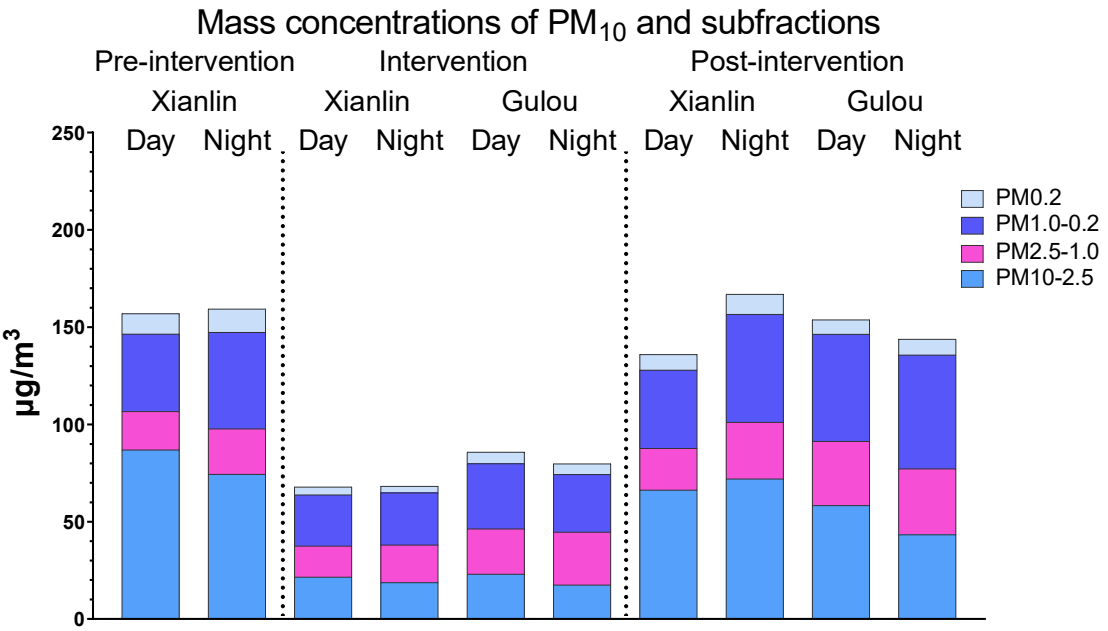

Figure 2: Mass concentrations of collected PM_{10} and subfractions in air, back-calculated from HVCI samples.

3.2.Air quality

The air mass concentrations of PM_{10} and the studied subfractions, back calculated from the sample masses by HVCI, are illustrated in Figure 2. The improved air quality is evident by the 57% decrease in PM_{10} mass concentration during the intervention (Xianlin average 68.1 µg/m^3) compared to the pre-intervention campaign (average 158.2 µg/m^3); this level was also clearly lower than that of the post-intervention campaign (Xianlin average 151.4 µg/m^3). However, this reduction is largely due to the marked reduction of $PM_{10-2.5}$ mass concentration from preintervention average of 80.1 µg/m^3 down to Xianlin intervention average of 20.0 µg/m^3; the changes in mass concentrations for the smaller PM fractions were not as striking. Conversely, the marked reduction of $PM_{10-2.5}$ mass concentration led to elevated relative contributions of $PM_{2.5-1.0}$ and $PM_{1.0-0.2}$ to total PM_{10} during the intervention, as shown in Table 2.

The mass percentages out of the total PM_{10} were the highest for $PM_{2.5-1.0}$ during the intervention meaning that this fraction was essentially enriched in the urban PM mixture, even though the absolute amount of PM was reduced. Indeed, $PM_{2.5}$ exhibited only slightly lower mass concentration during the intervention (Xianlin average 17.8 µg/m^3) in comparison with the pre-intervention (average 21.7 µg/m^3) and post-intervention campaigns (Xianlin average 24.9 µg/m^3). For $PM_{1.0-0.2}$, similar pattern of elevated relative amount during the intervention was observed for

Table 2: Mass percentages for the collected PM size fractions of total collected PM_{10}. Bold numbers indicate maximal values within each fraction.

	Pre-Intervention		Intervention				Post-Intervention			
	Xianlin		Xianlin		Gulou		Xianlin		Gulou	
	Day	Night	Day	Night	Day	Night	Day	Night	Day	Night
$PM_{0.2}$	6.65	**7.52**	5.93	5.00	6.90	6.81	5.91	6.16	4.84	5.65
$PM_{1.0-0.2}$	25.38	31.12	38.77	39.23	39.12	37.16	29.53	33.26	35.78	**40.67**
$PM_{2.5-1.0}$	12.56	14.68	23.45	28.38	27.14	**34.09**	15.77	17.41	21.44	23.53
$PM_{10-2.5}$	**55.41**	46.68	31.85	27.40	26.84	21.94	48.79	43.16	37.94	30.14

the Xianlin samples, whereas for Gulou, the relative amount of $PM_{1.0-0.2}$ showed no reduction after the intervention. $PM_{1.0-0.2}$ fraction can contain large contributions from long range transported PM, which could potentially overcome the beneficial effects of local emission restrictions, but this fraction also contains local emission particles that have grown out of the $PM_{0.2}$ size fraction by mechanisms such as agglomeration and coagulation. The relative amount of $PM_{0.2}$ remained relatively stable throughout the three sampling campaigns, whereas its mass concentrations showed a clear decrease from the pre-intervention level of 11.3 μg/m^3 down to 3.7 μg/m^3 in Xianlin during the intervention, and elevated to 9.0 μg/m^3 for the post-intervention campaign. For Gulou, the intervention $PM_{0.2}$ mass concentration (5.7 μg/m^3) was only slightly lower than the corresponding post-intervention campaign (7.8 μg/m^3). This could be attributed to the relatively stable emissions from coal and industrial combustion, the main factors in $PM_{0.2}$ composition as discussed in section 3.3, which were rather slightly restricted during the intervention. The changes in air mass trajectories and atmospheric processes as well as secondary aerosols can also influence the proportions of different PM size fractions. Furthermore, traffic remained dense in Gulou throughout the three sampling campaigns and its contribution to PM_{10} composition was elevated during the air quality intervention as depicted in Figure 3. Despite exhibiting a clearly smaller contribution to $PM_{0.2}$ than coal and industrial combustion, traffic was the second most important emission source in $PM_{0.2}$. In contrast, traffic was the least important of the identified emission sources in Xianlin. These factors could explain the relatively modest changes in $PM_{0.2}$ concentrations in Gulou.

The back-calculated average $PM_{2.5}$ concentrations of 47.9 μg/m^3 in Xianlin and 62.5 μg/m^3 in Gulou generally agree with the average $PM_{2.5}$ mass concentration of 61.4 μg/m^3 reported for the intervention period (Li et al. 2016). In our previous studies, the back-calculated mass concentrations based on HVCI samples were adequately in line with online measurements.

Overall, the air quality intervention approximately halved the airborne mass concentration of PM_{10}, an effect primarily affected by a dramatic decline of $PM_{10-2.5}$ fraction. Consequently, $PM_{2.5}$ mass concentration was only slightly reduced, although the secondary aerosols, long-range transport, and atmospheric processes naturally influence the PM levels as well.

3.3.PM source apportionment and chemical composition

We identified four principal components (PC 1-4), presented in Table 3, which explained 84.3 % of the total variance in the chemical composition of collected PM samples. PC1 explained 42.4 % of the variance; PC2 explained 17.0 %, whereas PC3 and PC4 explained 13.3 and 11.6 %, respectively. The high loading values of As, Pb, SO_4^{2-}, and a wide selection of heavy molecular weight PAHs in conjunction with moderate loading values for Cd, Mn, and Zn led us to identify PC1 as emissions from coal combustion and industry. We interpreted PC2 as emissions from traffic and oil or fuel combustion due to high loading values for Cr, Ni, Mn, and Fe, and moderate loadings for Mg, V, and NO_3^-; accordingly, this PC likely represents a mix of combustion and mechanically derived particles. This PC may also contain industrial and shipping emissions as well; the combination of Cr, Ni, and Fe suggests emissions from metalworking industry involving stainless steel. We assigned PC3 to soil dust due to the high loadings of well-established crustal components Al and Fe. This PC also contained the least loadings for PAHs and a high loading value for other trace metals, many of which usually occur in earth crust, supporting the interpretation. The loadings for Na and Cl^- also suggest a possible influence of long range transported sea spray particles. This together with V, Mn, and NO_3^-, possibly from shipping emissions, proposes that marine aerosols influenced this PC. High loadings for

Cd, Pb, NO_3^-, Zn as well as K and some heavy molecular weight PAHs led us to interpret PC4 as biomass combustion. However, the combination of Pb, Zn, and V could also be attributed to industrial or shipping emissions, but with the current dataset we are unable to distinguish these sources.

Table 3: Principal components explaining the variance in chemical composition of size-segregated PM obtained by PCA. Variables with factor loadings greater than 0.6 are in bold. Variables with factor loadings greater than 0.6 but with a higher factor loading in another PC are in bold italics. Variables with factor loadings less than 0.6 and present with higher loading in another PC are in

	PC 1		PC 2		PC 3		PC 4	
	Coal and industrial emissions		Traffic and oil/fuel combustion		Soil dust		Biomass combustion	
Inorganics	**As**	**SO_4^{2-}**	**Cr**	**Mn**	**Al**	**Fe**	**Cd**	**Pb**
	Na	K	**Ni**	***Fe***	**Cl^-**	**Mg**	**NO_3^-**	**Zn**
	Pb	*Mn*	*Mg*	*V*	V	*Mn*	*K*	*V*
	Cd	*Zn*	*NO_3^-*		*Na*	*NO_3^-*	*Cl^-*	
					Other trace metals			
PAHs	**BaA**	**CcP**	**1MPhe**	**Flu**	*Phe*		Nap	*BbF*
	BaP	**Chr**	**Ant**	**Phe**	*Ant*		*BaA*	*BcP*
	BbF	**Cor**	**Flr**	***Pyr***	*Flr*		*BaP*	*Per*
	BcP	**DaA**		*Nap*				
	BeP	**IcP**						
	BgP	**Per**						
	BjF	**Pyr**						
	BkF	**TPh**						
	1MPhe	*Flr*						
	Flu	*Nap*						

Figure 3 illustrates the influence of each PC in PM size fractions, sampling campaigns (pooled PM_{10} dataset), and locations (pooled PM_{10} dataset). PC2 and PC3 dominated the $PM_{10\text{-}2.5}$ fraction, where the least influence was observed for PC1; this indicates that soil dust and the possible marine aerosols discussed above, were the most important emission sources in this fraction together with traffic and fuel combustion. This reflects that particles in this size fraction are usually of local origins in calm conditions due to their fast settling and deposition, but they can be carried very long distances by strong winds such as during dust storms. Furthermore, traffic and construction produce mechanically generated coarse mode particles. In comparison, biomass (PC4) as well as coal and industrial combustion processes (PC1) contributed very little to the composition of $PM_{10\text{-}2.5}$.

Contrastingly, biomass combustion (PC4) was the leading emission source influencing the composition of $PM_{2.5\text{-}1.0}$, where the other sources showed low contributions. Biomass combustion was the most important contributor in $PM_{1.0\text{-}0.2}$ as well, whereas the relative contributions of traffic, fuel combustion, and soil dust showed were lower than in $PM_{2.5.1.0}$; coal and industrial combustion emissions displayed a similar level of contribution as in $PM_{2.5\text{-}1.0}$. These results agree well with the fact that $PM_{2.5\text{-}1.0}$ contains the smaller range of mechanically generated coarse mode particles, leading to higher contributions of traffic and soil dust sources in $PM_{2.5\text{-}1.0}$ compared to $PM_{1.0\text{-}0.2}$, which largely comprises aged combustion and secondary particles. The high factor values of biomass combustion in these two size fractions suggest that the biomass combustion emissions during the sampling campaigns were likely from both local and distant origins. The air mass trajectories, discussed in section 3.1, of the pre-intervention and post-intervention campaigns support the involvement of distant emissions, whereas during the intervention campaign, the air masses were

much closer to Nanjing during the last 120 h, which mitigates the impact of long-range transport of aerosols and emphasizes the local emission sources.

Finally, the predominant contributors to $PM_{0.2}$ composition were coal and industrial combustion emissions with low contributions from the other PCs. This indicates that the local combustion emissions were mostly from coal combustion, such as power generation, and industrial combustion processes, whereas biomass burning was negligible compared to biomass burning contributions in $PM_{2.5\text{-}1.0}$ and $PM_{1.0\text{-}0.2}$.

During the pre-intervention campaign, soil dust and biomass combustion showed the greatest contributions to the total PM_{10} composition, whereas coal and industrial combustion contributed slightly less; the influence of traffic and fuel combustion was the lowest in this campaign by a large margin. For the intervention and post-intervention campaigns, the influence of coal and industrial combustion emissions increased compared to pre-intervention. During the intervention campaign, the contribution of traffic and fuel combustion increased dramatically making it the dominant factor; in contrast, the influence of biomass burning and soil dust was greatly diminished. In the post-

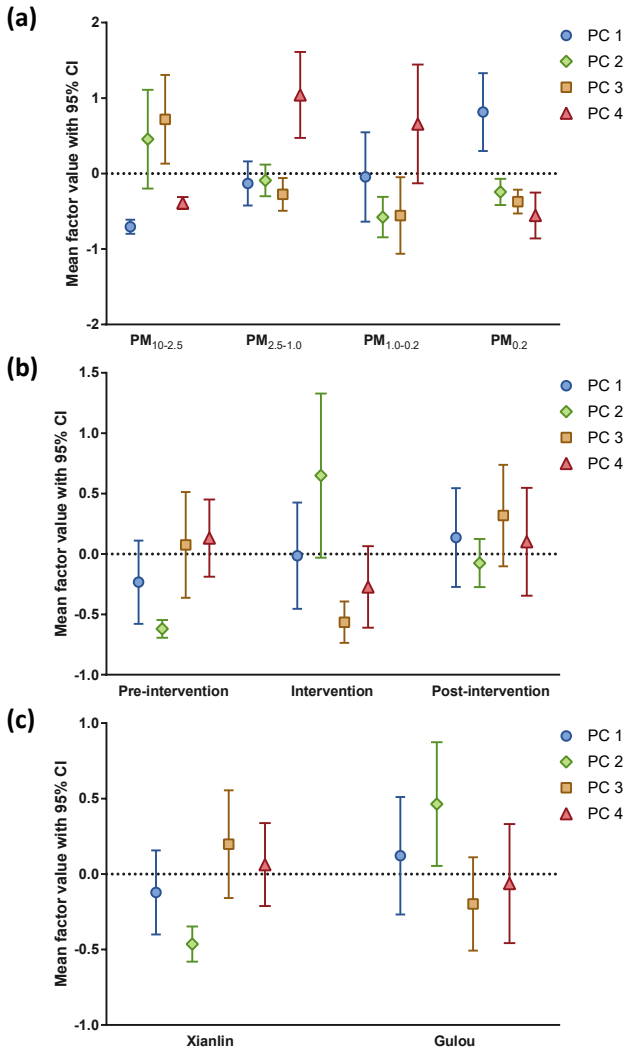

Figure 3: Mean factor values of the PCs obtained by PCA by PM size fraction (a), sampling campaign (b), and location (c). Mean with 95% CI.

intervention campaign, the contributions of the four emission sources were quite close, with the

smallest contribution observed for traffic and fuel combustion. These results indicate that the intervention and the changes in traffic due to the Youth Olympic Games greatly altered the emission profile in Nanjing by dramatically emphasized role of traffic emissions. Moreover, the restrictions on construction works during the intervention were successful in reducing the contribution of soil dust. Additionally, the amounts of airborne road dust were also controlled by frequent street washing. In contrast, the contribution of coal combustion and industrial emissions remained unaffected by the air quality control measures.

The comparison of factor values between sampling locations revealed that traffic and fuel combustion had a much larger contribution in Gulou compared to Xianlin, an unsurprising finding given the differences in traffic volume between downtown Nanjing and an urban background area. Differences between the sites for the other factors were rather low, but Gulou showed a slightly higher influence for coal combustion and industrial emissions than Xianlin, which can be attributed to the several industrial areas surrounding Gulou. In contrast, soil dust was a larger contributor in Xianlin than Gulou, which can indicate wind-blown dust from e.g. construction sites in the surroundings. Xianlin is generally upwind of Gulou and the local landscape with the 448-meter-high Purple Mountain between Xianlin and Gulou likely restricts the access of wind-blown dust to downtown Nanjing.

Time of day displayed very low differences in factor values with comparably large variations, but the influences of PCs 1-3 were higher in the night compared to day (data now shown); biomass combustion showed virtually no difference. This agrees with the fact that the night sample collection timeframe included the morning rush hour, and high pollution vehicles such as trucks were limited to operate at night. Moreover, night samples generally contained more PAHs than daytime samples owing to the lower mixing layer depth; additionally, lower temperatures and higher relative humidity at night facilitate PAH apportionment into the particle phase due to mechanisms such as condensation. The calmer weather with gentler winds at night also allows the PAHs to accumulate in the mixing layer better than during the generally windier daytime.

The chemical composition of the size-segregated PM fractions was measured separately for day and nighttime samples. The mass concentrations (μg/mg of PM mass) of the total inorganics, inorganic ions, metals, organic carbon (OC), elemental carbon (EC), and OC/EC ratio are shown in Table 4. Briefly, the mass concentrations of particle-bound inorganics in general were the lowest in the pre-intervention samples for all size fractions. However, this was mainly due to the low mass concentrations of secondary ions, only partially offset by the high concentration of metals, compared to the intervention and post-intervention campaigns where secondary inorganic ions displayed much higher contributions to PM mass.

We measured the OCEC contents of primarily nighttime Xianlin samples from each campaign, due to the limited amount of sample material, to gain a location-specific series of data. The OC content for $PM_{10\text{-}2.5}$ and $PM_{2.5\text{-}1.0}$ was fairly similar, and both size fractions displayed the lowest nighttime OC content in the pre-intervention samples, slightly higher level for the intervention samples, and the highest OC content in the post-intervention samples. However, daytime samples exhibited larger OC contents compared to the corresponding night sample in both size fractions. For $PM_{1.0\text{-}0.2}$, the lowest OC content was observed for the nighttime intervention sample, a slightly higher level for the pre-intervention sample, and the greatest content again for the post-intervention sample. Overall, the greatest OC concentrations were observed for the $PM_{0.2}$ samples.

EC content was much lower in comparison to OC, especially for $PM_{10-2.5}$ and $PM_{2.5-1.0}$, and EC mass concentrations displayed generally clear reductions in the intervention samples. EC content in $PM_{1.0-0.2}$ and $PM_{0.2}$, in contrast, was clearly higher than the larger fractions, accentuating the different nature of the sub-micron particles, which are mainly formed as primary or secondary combustion emissions. In contrast, $PM_{2.5-1.0}$ contains the smaller range of the mechanically derived coarse-mode particles in addition to the largest of the combustion-derived particles. Finally, $PM_{10-2.5}$ consists primarily of coarse particles with possibly fine particles adsorbed onto their surface.

Intervention $PM_{10-2.5}$ and $PM_{2.5-1.0}$ displayed very high OC/EC ratios primarily due to the proportionally large reduction in EC content, whereas OC was not as strikingly affected. The sample material of $PM_{0.2}$ was insufficient to reliably analyze the OCEC content of the intervention and daytime samples; pre-intervention sample displayed a slightly lower OC content than the post-intervention sample.

Table 4: Mass concentrations (µg/mg) of inorganics, OC, and EC in PM fractions from each sampling campaign by location and time of day.

	$PM_{10-2.5}$										**$PM_{2.5-1.0}$**									
	Pre-intervention		Intervention				Post-intervention				Pre-intervention		Intervention				Post-intervention			
	Xianlin		Xianlin		Gulou		Xianlin		Gulou		Xianlin		Xianlin		Gulou		Xianlin		Gulou	
	Day	Night	Day	Night	Day	Night	Day	Night	Day	Night	Day	Night	Day	Night	Day	Night	Day	Night	Day	Night
Total inorganics	203.54	**311.09**	242.20	352.92	291.98	**359.49**	273.38	**504.78**	464.70	471.43	**357.72**	335.60	499.35	572.05	490.19	**580.05**	392.50	455.89	**552.32**	514.97
Cl^-	8.10	**14.72**	9.62	**11.96**	0.88	9.14	12.74	**23.14**	20.50	19.69	6.51	**22.99**	7.04	**9.91**	4.84	7.89	13.75	**19.01**	15.71	18.82
SO_4^{2-}	37.55	**47.62**	38.94	**65.22**	28.24	59.14	50.44	**90.86**	87.03	78.27	**211.73**	144.50	305.16	**324.32**	292.55	273.68	142.92	140.10	**199.44**	160.43
NO_3^-	83.00	**86.58**	120.19	**184.78**	135.29	172.04	96.46	**172.38**	171.29	168.50	94.46	**134.65**	145.54	202.70	111.70	**242.11**	183.33	227.23	241.81	**249.20**
Metals	71.39	**157.74**	71.65	89.18	**124.64**	116.98	109.76	**210.07**	179.82	198.78	**43.25**	31.95	40.41	34.36	**79.96**	55.24	50.65	66.29	**92.58**	82.84
OC	N.A.	127.17	188.00	146.52	N.A.	N.A.	N.A.	225.40	N.A.	N.A.	204.43	111.23	N.A.	121.82	N.A.	N.A.	N.A.	198.25	N.A.	N.A.
EC	N.A.	11.54	4.58	3.57	N.A.	N.A.	N.A.	20.92	N.A.	N.A.	16.35	11.99	N.A.	5.59	N.A.	N.A.	23.00	20.83	N.A.	N.A.
OC/EC ratio	N.A.	11.02	41.07	41.10	N.A.	N.A.	N.A.	10.77	N.A.	N.A.	12.51	9.28	N.A.	21.80	N.A.	N.A.	N.A.	9.52	N.A.	N.A.
Total analyzed	203.54	**449.80**	434.78	**503.01**	291.98	359.49	273.38	**751.10**	464.70	471.43	**578.50**	458.82	499.35	**699.46**	490.19	580.05	415.50	**674.96**	552.32	514.97

	$PM_{1.0-0.2}$										**$PM_{0.2}$**									
	Pre-intervention		Intervention				Post-intervention				Pre-intervention		Intervention				Post-intervention			
	Xianlin		Xianlin		Gulou		Xianlin		Gulou		Xianlin		Xianlin		Gulou		Xianlin		Gulou	
	Day	Night	Day	Night	Day	Night	Day	Night	Day	Night	Day	Night	Day	Night	Day	Night	Day	Night	Day	Night
Total inorganics	399.91	**433.06**	413.70	495.32	499.51	**535.86**	453.04	**614.39**	496.99	531.72	**396.82**	332.83	46.65	348.22	373.90	**407.56**	**451.87**	351.22	350.21	413.36
Cl^-	2.66	**27.00**	2.42	**5.80**	1.44	4.04	9.69	**24.55**	1.12	15.95	1.41	**8.48**	N.A.	1.86	**4.51**	0.92	4.72	8.17	6.02	**11.06**
SO_4^{2-}	**301.31**	220.00	298.70	299.11	**388.89**	294.87	204.93	223.45	**226.40**	203.07	**329.41**	187.88	N.A.	282.49	228.40	**311.22**	**298.11**	183.33	213.09	226.49
NO_3^-	87.34	**135.00**	86.58	151.79	77.78	**205.13**	204.93	**332.41**	231.46	266.26	14.12	**59.39**	N.A.	12.99	**54.32**	50.00	88.68	**124.44**	80.63	123.84
Metals	8.15	**50.14**	25.49	**37.98**	30.71	30.53	32.66	31.18	35.49	**43.94**	50.03	**76.09**	46.16	49.34	**85.88**	44.76	**58.53**	34.12	48.71	49.89
OC	N.A.	170.84	N.A.	157.13	N.A.	N.A.	162.99	277.40	N.A.	N.A.	N.A.	241.51	N.A.	N.A.	N.A.	N.A.	N.A.	286.44	N.A.	N.A.
EC	N.A.	41.17	N.A.	23.95	N.A.	N.A.	N.A.	36.77	N.A.	N.A.	N.A.	40.95	N.A.	N.A.	N.A.	N.A.	N.A.	46.13	N.A.	N.A.
OC/EC ratio	N.A.	4.15	N.A.	6.56	N.A.	N.A.	N.A.	7.54	N.A.	N.A.	N.A.	5.90	N.A.	N.A.	N.A.	N.A.	N.A.	6.21	N.A.	N.A.
Total analyzed	399.91	**645.07**	413.70	**676.40**	499.51	535.86	616.04	**928.56**	496.99	531.72	396.82	**615.29**	46.65	348.22	373.90	**407.56**	451.87	**683.79**	350.21	413.36

Bold numbers indicate maximal values within the sampling campaign in each size range. N.A. = not analyzed.

3.3.1. Inorganics

Analyzed inorganic fractions of the total PM mass correspond to 20.4-50.5% of PM mass for $PM_{10-2.5}$ samples, 33.6-58.0% of PM mass for $PM_{2.5-1.0}$ samples, 34.0-61.4% of PM mass for $PM_{1.0-0.2}$ and 33.3-45.2% of PM mass for $PM_{0.2}$ samples (anions were not analyzed from intervention day sample from Xianlin). When taking OCEC into account, the analyzed fraction corresponded to 43-75% of PM mass for $PM_{10-2.5}$ samples, 46-70% of PM mass for $PM_{2.5-1.0}$ samples, 62-93% of PM mass for $PM_{1.0-0.2}$ samples and 62-68% of PM mass for $PM_{0.2}$ samples. SO_4^{2-} and NO_3^- were the main inorganic compounds analyzed from the samples, indicating strong contribution of secondary aerosols in the PM. SO_4^{2-} was the main inorganic compounds analyzed from the fine particle fractions ($PM_{0.2}$, $PM_{1-0.2}$ and $PM_{2.5-1}$), whereas NO_3^- was most abundant in the size fractions $PM_{1-0.2}$, $PM_{2.5-1}$ and $PM_{10-2.5}$. In PC analysis SO_4 was also related to coal and industrial combustion and NO_3 to biomass combustion. Al, Ca, Fe and Mg were the main elements in coarse particle fraction ($PM_{10-2.5}$) similar to the previous study (Rönkkö et al. 2018) and in PC analysis (Table 3) Al, Fe and Mg were

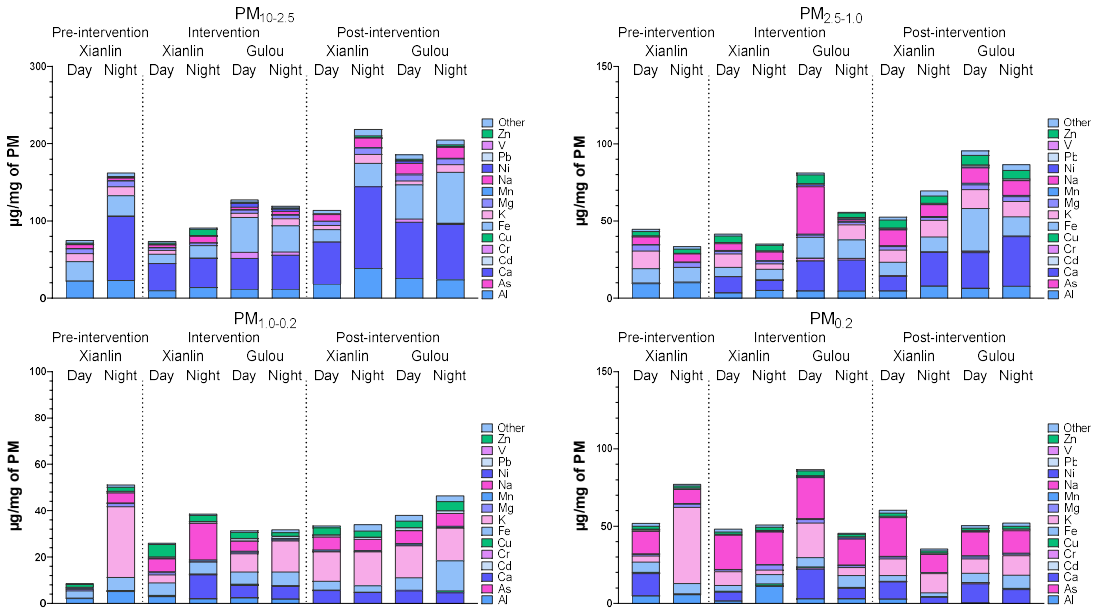

Figure 4: Mass concentrations of metal components in size-segregated PM.

associated to PC3 soil dust.

When comparing the samples between Gulou downtown and Xianlin background stations (intervention and post-intervention campaigns), there was more Fe in Gulou samples than in Xianlin samples in $PM_{0.2}$, $PM_{2.5-1}$ and $PM_{10-2.5}$ fractions, as illustrated in Figure 4. In PC analysis Fe was associated especially to traffic and oil/fuel combustion and the difference is likely due to higher traffic emission contribution in the Gulou station. In addition, during YOG the samples collected from Gulou contained more Cr and Ni than samples collected from Xianlin in all particle size fractions. Also Qi et al. observed enhanced Cr concentrations in Nanjing $PM_{2.5}$ during the YOG and suggested opaque steel and dye processes as well as automobile parts and aluminum and titanium alloys as the potential Cr sources (Qi et al. 2016). Since Cr in the current samples is substantially enriched in $PM_{10-2.5}$ and $PM_{2.5-1.0}$ from downtown Nanjing, it is likely generated in mechanical processes suggesting traffic and local metallurgic industry as possible emission sources. Stainless steel production or metalworking can emit particulate Cr and Ni, and the large shipyard northwest of our Gulou sampling site could be a possible source of such mechanically formed PM.

The clearly seasonally specific features in the PM composition were the high potassium content in the night-time samples of $PM_{0.2}$ and $PM_{0.2\text{-}1}$ during the pre-intervention campaign, which was associated with the crop residue burning around Nanjing (Miettinen et al., 2019).

As displayed in Figure 5, zinc was the predominant toxic metal in all studied PM size fractions with especially high concentrations seen in the $PM_{10\text{-}2.5}$ intervention night and $PM_{1.0\text{-}0.2}$ intervention day samples from Xianlin. Previous studies of trace elements in Nanjing have attributed Zn to vehicular exhaust and smelting processes (Yang et al. 2013, Zhou et al. 2014), as well as ship emissions on the nearby Yangtze River and their antifouling painting emissions in the local shipyard (Zhang et al. 2014). The intervention showed little to no effect on Zn mass concentrations, thus it was likely from a source not severely affected by the emission restrictions. This corresponds well with the observed high contribution of traffic emissions during the intervention.

Lead was another prominent toxic metal in the $PM_{2.5}$ particles. There are several metallurgic and mining industries in the vicinity of Nanjing, many of which are likely sources of particle-bound Pb. For $PM_{2.5\text{-}1.0}$ and $PM_{1.0\text{-}0.2}$, its mass concentration was slightly higher in the intervention samples compared to pre-intervention samples, but the greatest Pb concentrations were seen for the post-intervention samples. This follows the pattern of PC1, coal and industrial combustion emissions (Figure 3), in which Pb was present with a high loading value (Table 3). Yet, Pb was also present in PC4, biomass combustion, which showed the greatest contributions to $PM_{2.5\text{-}1.0}$ and $PM_{1.0\text{-}0.2}$ composition. In $PM_{0.2}$, however, Pb mass concentrations were the lowest in the intervention samples. Somewhat contrary to our findings, Li et al. reported almost halved Pb concentration in $PM_{2.5}$ during the YOG emission control period with the largest source of Pb during that timeframe being coal combustion (Li et al. 2016). They also observed that non-YOG $PM_{2.5}$ contained Pb from smelting activities as well. Interestingly, the change in emission sources reportedly changed the speciation of Pb and led to different bioavailability. The different bioavailability can cause differences in toxicological responses, and this effect is likely to apply for other multi-source chemical constituents as well.

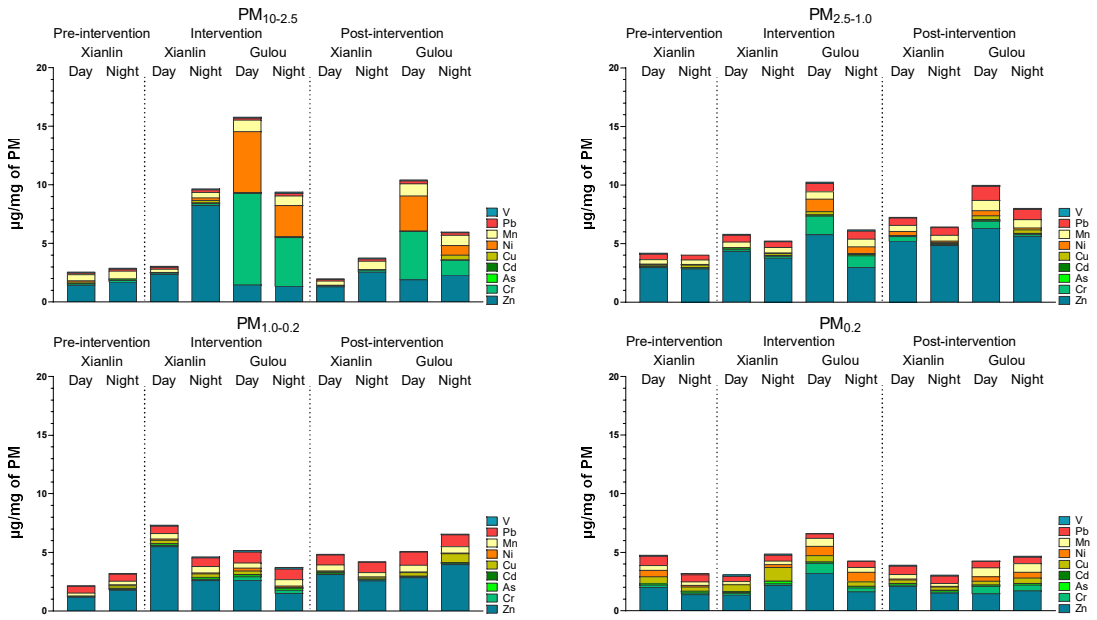

Figure 5: Mass concentrations of toxic metals in size-segregated PM.

3.3.2. PAHs

Huom! Sadenäytteissä oli melko paljon PAH:ja kuiviin näytteisiin verrattuna – vääristääkö niiden poisjättäminen tuloksia (jos muissa kampanjoissa näytteitä on kerätty joka säällä?

3-ring PAHs dominated the coarse particle fraction ($PM_{10-2.5}$), and 4-ring PAHs fine particle fractions ($PM_{0.2}$ and $PM_{1-0.2}$). Both 3-ring and 4-ring PAHs were abundant in $PM_{2.5-1}$. 5-ring and 6-ring PAHs were more abundant in fine particles fractions ($PM_{0.2}$ and $PM_{1-0.2}$) than in coarse particles, as in previous studies (Jalava et al. 2015). The mass concentrations of particle-bound PAHs are illustrated in **Error! Reference source not found.**. Phenanthrene, fluoranthene and pyrene were the most abundant PAH compounds in most of the samples, as in previous studies (Rönkkö et al. 2018). Nighttime samples contained mainly more PAHs than the corresponding daytime samples, similar to our previous observations (Jalava et al. 2015, Rönkkö et al. 2018).

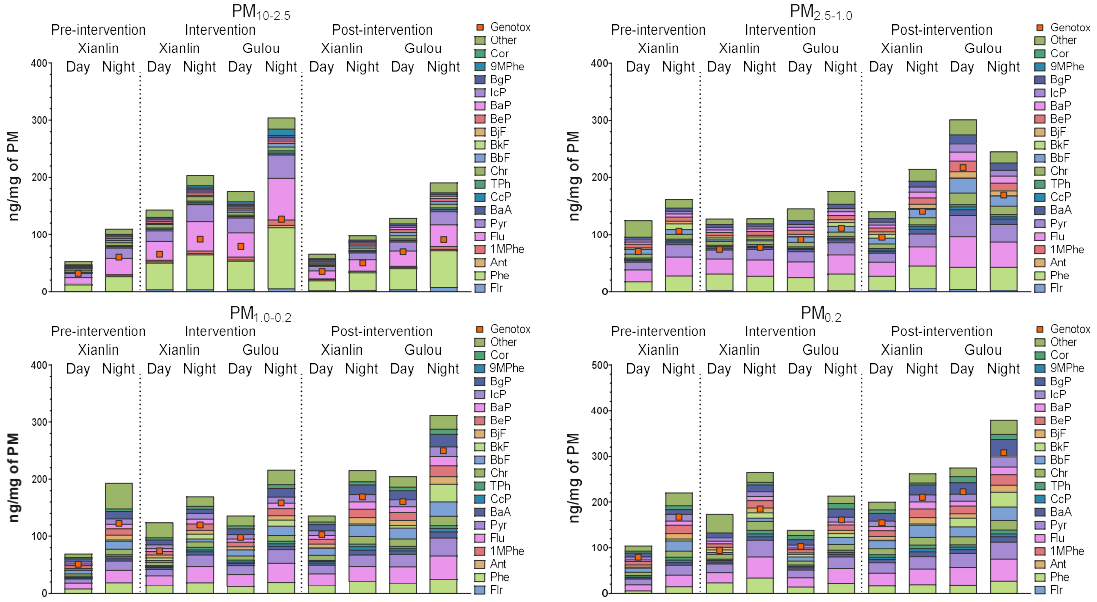

Figure 6: Mass concentrations (ng/mg) of PAHs and the sum of genotoxic PAHs in size-segregated PM.

In PC analysis, PAHs were mainly associated to PC1 coal and industrial emissions and PC2 traffic and oil/fuel combustion. Diagnostic ratios were calculated to further elucidate the emission sources. Ratio Flut(Flut+Pyr) was between 0.55-0.63 and indicates grass, wood and coal combustion rather than liquid fossil fuel combustion (Yunker et al. 2002) as in previous studies (Rönkkö et al. 2018) and as in the study concerning the quartz filter samples collected the same time than the samples used in this study (Miettinen et al. 2018). The ratio was the highest in coarse $PM_{10-2.5}$ fraction (0.63) and the lowest in ultrafine $PM_{0.2}$ fraction (0.55), indicating that the source of the smallest $PM_{0.2}$ fraction is closer to liquid fossil fuel combustion than the sources of the coarse size fraction. BaP/(BaP+BeP) varied between 0.37-0.46 (Figure 7), being close to values reported by Miettinen et al. (2018) (0.29-0.51) and indicating partial photolysis of particles instead of completely fresh emissions (Kang et al. 2017, Oliveira et al. 2011). The ratio was lower in ultrafine fraction (0.38) than in other size fractions (0.43-0.45), indicating higher contribution of aged particles in ultrafine fraction. The ratios were slightly higher in nighttime samples than in daytime samples, indicating higher contribution of fresh emissions in nighttime. Ratio IcP/(IcP+BgP) was between 0.41-0.47

(Figure 7) indicating petroleum combustion (Yunker et al. 2002, Wang et al. 2017, Miettinen et al. 2018). BgP/BeP varied between 0.74-1.30 (Figure 7), indicating more coal combustion than vehicular emissions (Ohura et al. 2004, Wang et al. 2009). The ratio was highest in the ultrafine fraction (1.30) and lowest in the coarse fraction (0.74), indicating higher contribution of the vehicular emissions in the ultrafine particles. BaA/(BaA+Chr) varied between 0.38-0.46 (Figure 7) in $PM_{0.2}$, $PM_{1.0-0.2}$ and $PM_{2.5-1.0}$, indicating combustion and vehicular source, and 0.34 in coarse fraction $PM_{10-2.5}$, indicating petroleum or combustion source (Li et al. 2012, Yunker et al. 2002). DahA/Flu was between 0-1.20 (Figure 7), indicating the mixture of the sources. The ratio was lower in the coarse fraction (0.12) than other size fractions (0.56-1.2), indicating the source of the coarse particles being closer to diesel and gasoline combustion than the source of the smaller particles (Fu et al. 2010). BgP/IcP varied between 1.14-1.50 (Figure 7), indicating industrial coal combustion and diesel exhaust emissions(Li & Kamens 1993, Ohura et al. 2004, Yu et al. 2011, Zhang et al. 2008).

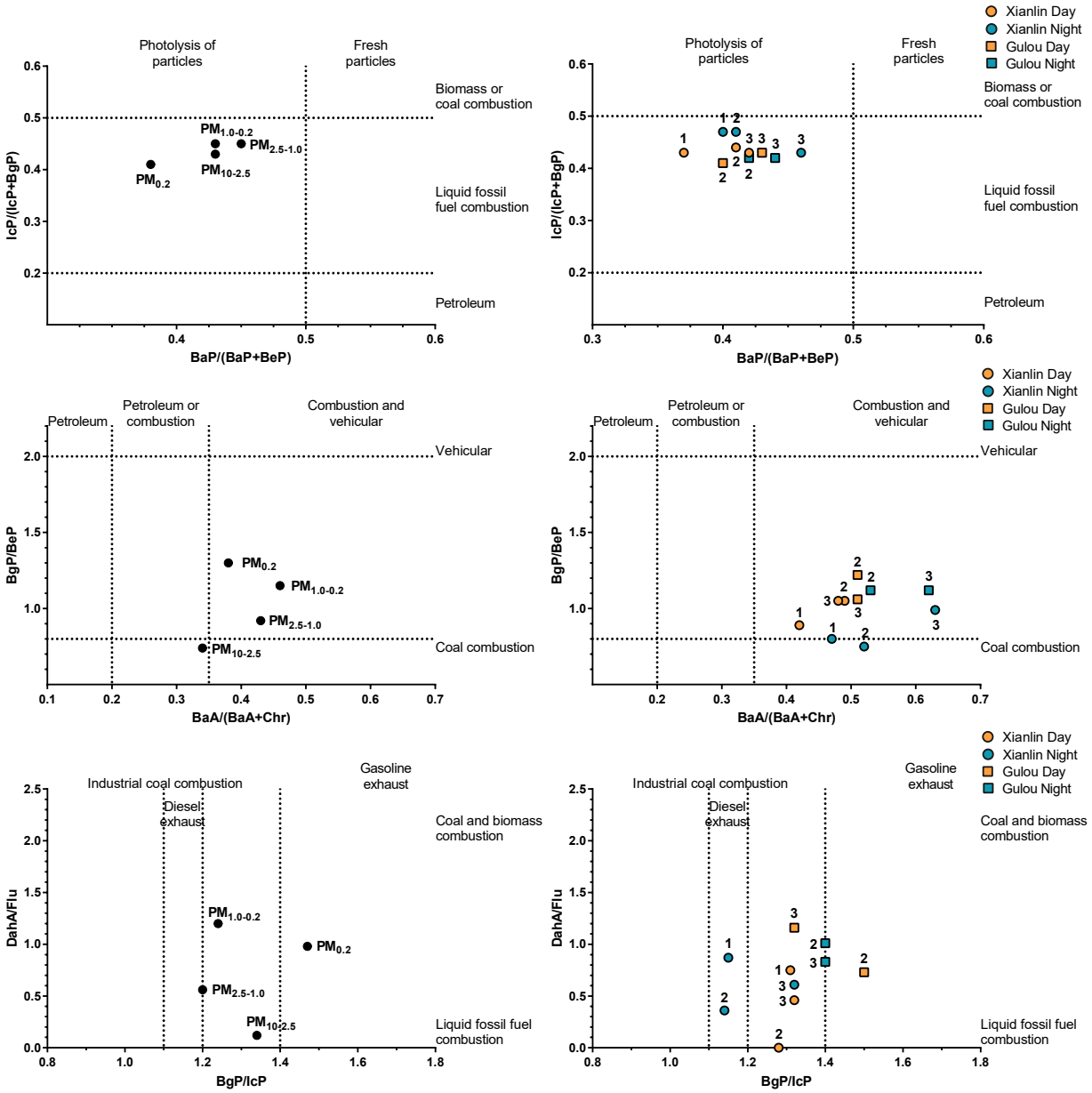

Figure 7: Diagnostic ratios of PAHs used to identify possible emission source contributions in the collected PM. Left pane displays diagnostic ratios for size-segregated PM fractions, whereas right pane shows diagnostic ratios for PM_{10} by sampling campaign, location, and time of day. 1 = pre-intervention, 2 = intervention, 3 = post-intervention campaign. BaP/(BaP+BeP)[a] (Kang et al. 2017, Oliveira et al. 2011), IcP/(IcP+BgP)[b] (Wang et al. 2017, Yunker et al. 2002), BaA/(BaA+Chr)[c] (Li et al. 2012, Yunker et al. 2002), BgP/BeP[d] (Ohura et al. 2004, Wang et al. 2009), BgP/IcP[e] (Li & Kamens 1993, Ohura et al. 2004, Yu et al. 2011, Zhang et al. 2008), DahA/Flu[f] (Fu et al. 2010).

3.4.Toxicological analyses

3.4.1. Cytotoxicity – loss of cellular metabolic activity and cell membrane integrity

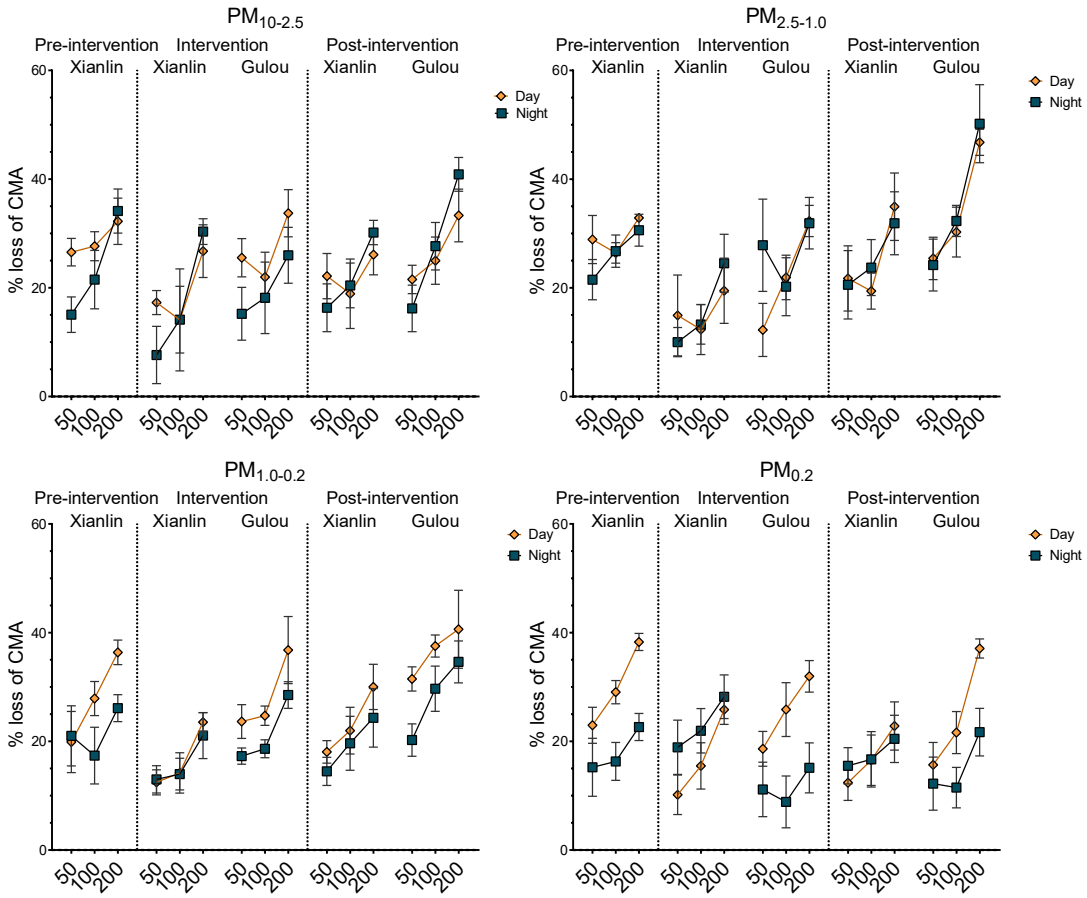

Figure 8: Loss of cellular metabolic activity of PM-exposed co-cultures, expressed as percentage of CMA lost compared to untreated control. These data show the measured CMA responses prior to being utilized as input for the factorial linear multiple regression models, which provided the estimated means and regression parameter estimates allowing the assessment of the effects of sampling campaign, location, and time of day. Mean ± SEM, n = 4.

All PM size fractions caused dose-dependent decreases in cellular metabolic activity (CMA), indicating disturbance of cellular function caused by PM (Figure 8). Filter blanks from different sampling locations did not elicit significantly different responses for cellular metabolic activity, thus formal comparisons between sampling locations are possible. No changes in cell membrane integrity or cellular viability were observed by PI exclusion and DAPI assays for any of the PM fractions (data not shown), indicating that the PM exposure did not cause necrosis in the co-culture model.

To assess the effects of sampling campaigns, sampling location, and time of day on the observed variation in the cellular metabolic activity, we performed factorial multiple linear regression analysis by general linear model with CMA response as continuous dependent variable, campaign, location, and time of day as categorical fixed effects and exposure dose as continuous covariate. The full results tables of the multiple linear regression models are presented in the supplementary material.

$PM_{10\text{-}2.5}$

For the $PM_{10\text{-}2.5}$ fraction, the loss of CMA was affected differently depending on the main effects of campaign (p = 0.009), sampling location (p = 0.010), and time of day (p = 0.001). Furthermore, the regression slopes for the day samples were on average slightly less steep than the night sample slopes, as indicated by the significant interaction term of time of day and exposure dose (p = 0.008).

Table 5: Estimated means of lost CMA for $PM_{10\text{-}2.5}$ produced by the factorial multiple linear regression model.

			Mean loss of		95% Confidence Interval	
Campaign	Location	Time of day	CMA (%)	Std. Error	Lower Bound	Upper Bound
Pre-intervention	Xianlin	Day	27.714	1.898	23.954	31.474
		Night	24.643	1.871	20.936	28.350
Intervention	Xianlin	Day	20.881	1.679	17.553	24.209
		Night	17.809	1.657	14.526	21.093
	Gulou	Day	25.317	1.653	22.040	28.593
		Night	22.245	1.646	18.984	25.506
Post-intervention	Xianlin	Day	24.234	1.653	20.957	27.510
		Night	21.162	1.646	17.901	24.423
	Gulou	Day	28.670	1.646	25.408	31.931
		Night	25.598	1.653	22.321	28.874

Estimated means evaluated at mean dose value 116,95 µg/ml

After adjusting for the dose, we observed a 24.1 % (95% CI: 4.6, 43.5 %) reduction in the loss of CMA during the intervention compared to pre-intervention campaign. The post-intervention loss of CMA was in-between the former two, showing a mean increase in loss of CMA of 15.6 % (95% CI: -3.5, 34.6) from the intervention level. $PM_{10\text{-}2.5}$ from Gulou caused 19.5 % (95% CI: 4.7, 34.3) greater loss of CMA compared to Xianlin. As noted above, the estimated means exhibited in Table 5 for time of day are not a completely reliable way to assess the differences in effects between night and daytime $PM_{10\text{-}2.5}$; the daytime $PM_{10\text{-}2.5}$ caused 13.1 % (95% CI: 0.3, 26.0) greater loss of CMA percentage at the evaluated dose of 116.95 µg/ml used in the model. However, the day and night regression slopes intercept at dose value of 163.58 µg/ml, and the regression slope for the night samples was over twice of that for day, indicating a much higher rate of dose-dependent increase in lost CMA. According to the regression model, the day samples produce higher responses of lost CMA below this dose due to the higher elevation of the regression line, whereas above this dose the steeper increase for the night samples overcomes the different elevation.

In summary, these results indicate that the air quality intervention reduced the cytotoxic effect of $PM_{10\text{-}2.5}$ on cellular metabolic activity, but this beneficial effect was somewhat diminished in the post-intervention samples. The campaign factor caused the largest variations in the cellular metabolism of $PM_{10\text{-}2.5}$-exposed cells, followed by the effect of location. The results also suggest a greater cytotoxic effect for the $PM_{10\text{-}2.5}$ collected in dense urban environment at the downtown Gulou sampling site compared to the urban background location at Xianlin. Furthermore, daytime $PM_{10\text{-}2.5}$ displayed higher initial cytotoxic potential, but this difference would be offset at doses above 163 µg/ml, where the more pronounced incline of the dose-response profile for the nighttime $PM_{10\text{-}2.5}$ would lead to greater responses.

$PM_{2.5\text{-}1.0}$

In the regression model for $PM_{2.5\text{-}1.0}$, the campaign factor displayed a significant effect ($p = 7.393 \times 10^{-8}$) indicating that $PM_{2.5\text{-}1.0}$ from different campaigns caused distinct CMA responses. Location ($p = 0.496$) and time of day ($p = 0.707$) showed no significant effects, suggesting that they had at best minor influence on the elevations of the regression lines in the model. However, the significant interaction term of location and dose ($p = 0.046$) indicated a difference in the slopes of the regression model, and therefore dose-response profiles, between Xianlin and Gulou. Indeed, the slope for Xianlin samples was almost half of that for Gulou samples, which means that the CMA lost due to PM exposure increased by almost double the rate in Gulou compared to Xianlin for each 1 µg/ml dose increment. The regression lines for Xianlin and Gulou did not intercept with realistic exposure doses; essentially, the Gulou $PM_{2.5\text{-}1.0}$ showed greater baseline cytotoxic response on CMA and a more rapidly growing response with increasing dose in comparison with Xianlin.

Table 6: Estimated means of lost CMA for $PM_{2.5\text{-}1.0}$ produced by the factorial multiple linear regression model.

		Time of			95% Confidence Interval	
Campaign	Location	day	Mean loss of CMA (%)	Std. Error	Lower Bound	Upper Bound
Pre-intervention	Xianlin	Day	27.536	2.071	23.434	31.638
		Night	28.174	2.071	24.072	32.277
Intervention	Xianlin	Day	15.234	1.842	11.584	18.884
		Night	15.872	1.842	12.222	19.523
	Gulou	Day	24.305	1.842	20.655	27.955
		Night	24.943	1.842	21.293	28.594
Post-intervention	Xianlin	Day	25.275	1.842	21.625	28.926
		Night	25.914	1.842	22.264	29.564
	Gulou	Day	34.346	1.842	30.696	37.997
		Night	34.985	1.842	31.335	38.635

Estimated means evaluated at mean dose value 116.95 µg/ml

Table 6 displays the estimated means acquired by the regression model. After adjusting for the exposure dose, the intervention $PM_{2.5\text{-}1.0}$ showed remarkably low loss of CMA compared to pre- and post-intervention campaigns; loss of CMA for intervention was 38.0 % (95% CI: 19.3, 56.7) lower compared to pre-intervention PM, and 33,3 % (95% CI: 18.1, 48.5) lower compared to post-intervention. Gulou PM caused 39.4 % (95% CI: 23.2, 55.7) greater loss of CMA compared to Xianlin at the evaluated dose of 116.95 µg/ml; due to the greater regression slope for Gulou, this difference would increase with higher doses. There was, however, virtually no variation of CMA attributable to time of day.

Overall, we observed a clear reduction of $PM_{2.5\text{-}1.0}$-induced cytotoxicity via loss of cellular metabolic activity attributable to the air quality intervention. However, the loss of metabolic activity returned to near pre-intervention levels for the post-intervention PM. Furthermore, $PM_{2.5\text{-}1.0}$ from Gulou produced notably greater cytotoxic effects than Xianlin $PM_{2.5\text{-}1.0}$, whereas there was no definite day-night variation in the responses.

$PM_{1.0\text{-}0.2}$

The results for $PM_{1.0\text{-}0.2}$ obtained by the multiple linear regression model were straightforward compared to the other PM fractions. No significant interaction terms were observed and all factors

of campaign ($p = 1.1*10^{-6}$), location ($p = 6.4*10^{-9}$), and time of day ($p = 4.9*10^{-5}$) explained substantial amounts of variation in the loss of CMA response. This was the only fraction showing no interaction terms involving dose, which indicates that the slopes of the regression lines were virtually identical. This renders comparisons between the individual samples and of the main effects simple, since the mean differences remain the same regardless of the exposure dose.

A substantial attenuation in the loss of CMA response was observed for the $PM_{1.0\text{-}0.2}$ collected during the intervention compared to both pre-intervention (33.6 % lower, CI: 17.6, 49.6) and post-intervention campaigns (23.2 % lower, 95% CI: 9.2, 37.2); thus, the air quality intervention reduced the cytotoxic potential of $PM_{1.0\text{-}0.2}$, but this improvement was lost after the intervention period. Gulou $PM_{1.0\text{-}0.2}$ displayed drastically higher loss of CMA compared to Xianlin (45.7 % greater, 95% CI: 31.3, 60.1). Finally, daytime $PM_{1.0\text{-}0.2}$ proved somewhat more detrimental for CMA compared to particles collected at night (daytime mean 25.2 % higher, 95% CI: 13.3, 37.0). The estimated means

Table 7: Estimated means of lost CMA for $PM_{1.0\text{-}0.2}$-exposed co-cultures obtained by the multiple linear regression model.

		Time of			95% Confidence Interval	
Campaign	Location	day	Mean	Std. Error	Lower Bound	Upper Bound
Pre-intervention	Xianlin	Day	29.182	1.702	25.810	32.554
		Night	23.317	1.702	19.945	26.689
Intervention	Xianlin	Day	18.717	1.515	15.716	21.717
		Night	12.851	1.515	9.851	15.852
	Gulou	Day	28.474	1.515	25.474	31.474
		Night	22.609	1.515	19.609	25.609
Post-intervention	Xianlin	Day	24.954	1.515	21.953	27.954
		Night	19.089	1.515	16.088	22.089
	Gulou	Day	34.711	1.515	31.711	37.711
		Night	28.846	1.515	25.846	31.846

Estimated means evaluated at mean dose value 116,95 µg/ml

for the individual samples area presented in Table 7.

$PM_{0.2}$

The $PM_{0.2}$ dataset produced the most complex results in the factorial multiple regression model. In addition to significant main effect of campaign ($p = 0.019$) and non-significant main effects for location and time of day ($p = 0.642$ and $p = 0.357$, respectively), we observed three significant interaction terms. The result of the campaign factor establishes that the CMA responses differed between the campaigns even when the effects of the other factors were set to zero; time of day and location showed no such independent effects. The significant interaction between time of day and exposure dose ($p = 0.018$) again indicates the difference in regression slopes (slope over twice greater for daytime $PM_{0.2}$ compared to night), and thus different dose-response profiles for the daytime and night samples. Moreover, the interaction terms between time of day and campaign ($p = 0.0005$), and time of day and location ($p = 0.00001$) show that these factor combinations explain significant amounts of variance in the CMA response while expressing that the data do not support general trends that would hold true for every such combination. Instead, the effects were conditional, i.e. direction of the differences between estimated means were dependent on the combination of these factors. This is by no means an unexpected or controversial result, rather it

highlights that the influence of these factors on CMA response for $PM_{0.2}$ followed no general pattern.

Table 8: Estimated means of lost CMA for $PM_{0.2}$ obtained by the multiple linear regression model.

Campaign	Location	Time of day	Mean loss of CMA (%)	Std. Error	95% Confidence Interval	
					Lower Bound	Upper Bound
Pre-intervention	Xianlin	Day	30.099	2.160	25.817	34.381
		Night	18.064	2.160	13.782	22.346
Intervention	Xianlin	Day	17.437	1.878	13.715	21.160
		Night	20.529	1.878	16.807	24.251
	Gulou	Day	25.202	1.878	21.480	28.924
		Night	14.203	1.878	10.481	17.926
Post-intervention	Xianlin	Day	16.965	1.878	13.243	20.688
		Night	20.039	1.878	16.316	23.761
	Gulou	Day	24.730	1.934	20.897	28.564
		Night	13.713	1.934	9.881	17.546

Estimated means evaluated at mean dose value 116,95 µg/ml

The estimated means for the factorial effect of campaign displayed that the intervention samples caused 20.9 % lower loss of CMA (95% CI: 0.8, 40.9) compared to the pre-intervention samples; post-intervention produced 22.8 % (95% CI: 2.7,42.9) lower loss of CMA than pre-intervention. However, as shown in Table 8 and highlighted by the significant interaction term for campaign and time of day, this effect was true for the daytime samples, while nighttime samples displayed altogether dissimilar effect of a slightly lower loss of CMA for the pre-intervention campaign compared to the intervention and post-intervention campaigns. Thus, the cytotoxicity via loss of CMA was reduced during the air quality intervention only for the day samples, and it remained at that level even afterwards during the post-intervention campaign. This suggests that the air quality intervention was not the sole driving factor in reducing $PM_{0.2}$ cytotoxic potential. The different atmospheric processes and air mass origins during the post-intervention campaign, as discussed in section 3.1, likely have an effect on PM composition and the concomitant toxicological responses. In contrast, $PM_{0.2}$-induced loss of CMA was not affected by the air quality intervention for the nighttime samples, which is a highly interesting finding.

There was virtually no difference in the estimated means between Xianlin and Gulou); instead, a notable difference between day and night (day 35.5 % higher than night, 95% CI: 23.4, 47.5) was present. However, the significant interaction terms mentioned earlier render the interpretation of these figures alone misleading. Instead, the effects should be interpreted from the estimated means of individual samples presented in Table 8 while simultaneously considering the different regression slopes for the day and nighttime responses, which, as discussed earlier, implied a sharper dose-dependent increase in loss of CMA for daytime $PM_{0.2}$ compared to night. The regression lines for day and nighttime $PM_{0.2}$ from Xianlin intercepted approx. at dose of 174 µg/ml for the intervention and post-intervention campaigns, which indeed displayed lower estimated means for the daytime $PM_{0.2}$ compared to night at the estimated dose of 116.95 µg/ml. For these campaigns, at lower doses, the

responses for daytime $PM_{0.2}$ were lower, whereas for higher doses the responses for daytime $PM_{0.2}$ would be higher compared to night. For the other day-night pairings from corresponding campaigns and locations, daytime responses showed ubiquitously higher elevations and steeper inclines of dose-response, indicating that daytime $PM_{0.2}$ from Gulou in general and pre-intervention Xianlin produced higher baseline cytotoxicity via loss of CMA as well as more rapidly increasing loss of CMA with increasing exposure dose compared to corresponding nighttime $PM_{0.2}$. Furthermore, Table 8 shows that the loss of CMA was uniformly higher for daytime $PM_{0.2}$ from Gulou compared to Xianlin, and higher for nighttime $PM_{0.2}$ from Xianlin in comparison with Gulou; this contrast explains the observed significant interaction term between time of day and location.

Overall, the loss of CMA for $PM_{0.2}$ displayed rather complex differences primarily due to the effects of time of day, which confounded the effects of campaign and location while also showing more steeply increasing response profile for the day samples compared to nighttime $PM_{0.2}$. Intervention samples displayed a decreased level of cytotoxicity via loss of CMA only for the daytime $PM_{0.2}$; however, the corresponding post-intervention sample exhibited a similar level. Thus, the reduction in cytotoxicity was not attributable to the air quality intervention alone. Loss of CMA was also dependent on the location and time of day in a contrasting manner; for $PM_{0.2}$ collected during daytime, greater loss of CMA was observed for Gulou $PM_{0.2}$ compared to Xianlin, whereas for nighttime, Xianlin $PM_{0.2}$ proved more harmful.

3.4.2. Intracellular oxidative stress

As demonstrated in Figure 9, oxidative stress measured by DCF was clearly reduced during the intervention period for the PM size fractions able to elicit responses higher than control, i.e. $PM_{10\text{-}2.5}$ and $PM_{0.2}$. The response was especially high for pre-intervention $PM_{10\text{-}2.5}$ from Xianlin, though post-intervention samples from Gulou produced somewhat elevated response for oxidative stress as well. Post-intervention samples from Gulou induced slightly higher oxidative stress responses than the corresponding Xianlin samples for $PM_{10\text{-}2.5}$ and $PM_{2.5\text{-}1.0}$; we observed no difference between the

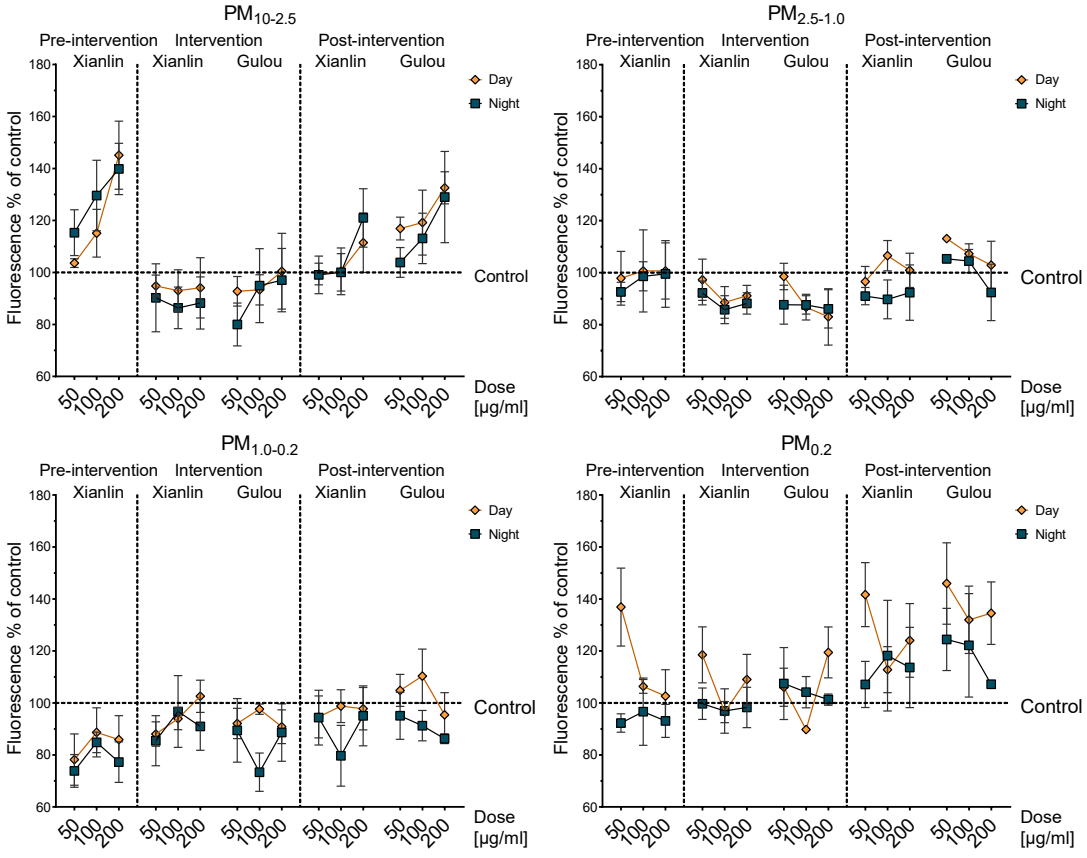

Figure 9: Oxidative stress responses of co-cultures exposed to size-segregated PM. Mean ± SEM, n = 4.

sampling sites for the intervention samples. Filter blanks from different sampling locations did not elicit different responses for intracellular oxidative stress, thus comparisons between sampling locations are possible.

Most interestingly, for $PM_{0.2}$ we observed that the day samples of pre-intervention and post-intervention campaigns caused high initial oxidative stress responses for the smallest exposure dose, highlighting their oxidative potential. However, the response decreased for the higher doses. These results are in stark contrast to our previous study where $PM_{0.2}$ showed no significant increases of oxidative stress in a monoculture of A549 cells, and the dose-response curves were very slightly increasing in contrast to the decreasing response profile of the current study (Rönkkö et al. 2018). Whether this difference is more due to the different biological responses owing to the incorporation of THP-1 cells into the current co-culture model or different composition of PM, is an issue we are unable to discern here. As discussed in section **Error! Reference source not found.**, coal and industrial combustion emissions dominated the $PM_{0.2}$ composition, which contained a complex mixture of harmful components including several toxic metals and a wide selection of PAHs. It is possible that some of these components or their combination modulate the oxidative stress response so that higher concentrations of the mixture produce lower responses. Lower exposure doses than the currently employed would also be an interesting avenue for further research in elucidating the oxidative effects of $PM_{0.2}$.

$PM_{10\text{-}2.5}$ composition was largely influenced by soil dust and traffic emissions; the contained notable amounts of transition metals, known for causing elevated oxidative stress responses (Viitteet), could account for these results. The diminished oxidative stress responses for the intervention samples could be linked to the decreased contribution of soil dust during the intervention, since the influence of traffic emissions was reduced during that time as discussed in section 3.3.

The low oxidative stress responses for $PM_{2.5\text{-}1.0}$ and $PM_{1.0\text{-}0.2}$ could be related to their ability to decrease cellular metabolic activity, thus reducing the level of normal metabolic-related oxidative stress in the cell; it is also possible that after 24 hours, their oxidative potential had already diminished. As discussed in section 3.3, the composition of $PM_{2.5\text{-}1.0}$ and $PM_{1.0\text{-}0.2}$ was dominated by biomass combustion emissions possibly from distant origins, which had aged during the long-range transfer of aerosols. This could lead to lowered chemical reactivity and oxidative potential for these size fractions.

3.5. Relationship between emission sources and chemical components on toxicological responses

As discussed in section 3.4, the toxicological endpoints displayed varying responses, and the campaigns, location and time of day influenced these variations. We also identified four principal components corresponding to four PM emission source groups by PCA. This was based on the chemical composition of the collected PM samples, which displayed distinct variations between PM size fractions, sampling campaigns, and locations as discussed in section 3.3. To assess the influence of these emission sources on the toxicological endpoints, we performed a mixed model analysis of the relationship between the observed toxicological responses and principal components. Sample size was insufficient for fraction-specific analyses; thus, the analyses were run with the combined dataset of chemical composition and toxicological responses of all PM size fractions. However, the effects of PM size, as well as location, were incorporated in the model as random effects, which

takes into account that the chemical composition of the samples was not independent within each level of these factors. They showed no significant random effects for the parameter estimates.

3.5.1. Cellular metabolic activity

The mixed model analysis of cellular metabolic activity and the principal components obtained from PCA revealed significant effects for exposure dose ($p = 0.044$) and time of day ($p = 0.002$); these results indicate that the responses were dose-dependent, and time of day caused substantial variation in the response. PC3 (soil dust) and PC4 (biomass combustion) displayed significant interaction terms with time of day ($p = 0.009$ and $p = 0.001$, respectively), indicating that their influence on the CMA response was different between daytime and night. Effects of PC1 (coal and industrial combustion) and PC2 (traffic and fuel/oil combustion) were not significant, but their interaction terms with exposure dose were retained in the model because they improved the model fit. When accounting for the random effects of PM size and sampling location due to non-independence of the samples within these factors, the parameter estimates suggest that PC3 increased loss of CMA twice more for the night PM_{10} (parameter estimate 3.278, 95 % CI: 1.216, 5.341) than daytime (1.650, 95 % CI: -1.191, 4.490). PC4 increased the loss of CMA slightly more with very similar estimates for day (3.247, 95 % CI: 1.149, 5.346) and night PM10 (3.545, 95 % CI: 1.593, 5.497). PC1 displayed a dose-dependent increase in the response of lost CMA, which was clearly stronger than the very modest dose-dependent increase due to PC2.

The comparison of changes in BIC value for the model with each PC removed separately revealed that the effect sizes for each PC were quite similar with the greatest effect size for PC4 (biomass combustion, 4.3 % change in BIC). PC3 (soil dust) had the second largest influence on CMA response (3.6 % BIC change), followed by PC1 (coal and industrial combustion, 3.1 % BIC change) and PC2 (traffic and fuel/oil combustion, 2.6 % BIC change). The similarity of effect sizes is likely largely due to the combined dataset used in the analysis, which masks the possible size fraction-specific effects of the PCs. Besides, some chemical components, such as Ca and Cu, were excluded from the dataset, since their sample sizes were too low for PCA. Overall, the analysis would be much stronger with sample sizes large enough to analyze size fractions separately; however, this is an improvement left for future studies.

The highest effect seen for PC4 emphasizes the influence of its most notable constituents, Cd, Pb, and Zn on adversely affecting the cellular metabolic activity of the employed cell model. PC3 contains a selection of typically crustal metals and also the sum of other analyzed trace metals, including rare earth metals, which displayed very low mass concentrations in the PM samples; the effect for PC3 suggests that Al, Fe, Mg and the other trace metals are indeed harmful for the cell model. Surprisingly, the crustal metals ranked higher than elements of PC1 and PC2 that are associated with coal and industrial combustion and traffic, emission sources widely regarded as the most harmful to human health. However, PC3 could also contain emissions from ship fuel oil combustion. These effects are linked to the factor values discussed in section 3.3**Error! Reference source not found.**, where PC3 and PC4 displayed decreased contributions during the intervention and higher influence during pre- and post-intervention; this correlates well with the generally lower loss of CMA during the intervention.

In contrast, PC2 displayed a strikingly dissimilar pattern with high contribution during the intervention and low influence during the other two campaigns; PC1 was virtually unaffected by the intervention and showed only little variance between the campaigns. This finding emphasizes the need to research the health effects of not only combustion-derived particles, but the larger

mechanically formed particles, for example soil and road dust, construction dust, etc. Even though the penetration of larger particles into the lower airways is restricted, they can cause harm in the upper airways and lead to health responses such as exacerbated asthma symptoms.

The mixed model analysis was also employed on a set of metals (Ca, Cu, K, Mg, Zn) to assess their individual effects on cellular metabolic activity. These metals were selected on a statistical basis and this analysis is unable to tell if these metals are the most important single components affecting the loss of CMA. Other metals and PAHs were excluded from the analysis due to their observed collinearity with other chemical components influencing CMA response, which violates an important assumption in the mixed model analysis. Among the metals in this analysis, Ca displayed the greatest effect on loss of CMA (13.9 % BIC change) and was closely followed by Mg (11.9 %), Cu (11.4 %), and Zn (10.7 %) while K displayed a clearly lower effect size (4.6 %). The high ranking of Ca and Cu, components not usable in the PCA analysis to form PCs, with effect sizes greater than Zn and K, which were incorporated in the PCs, suggests that the current PCs could be improved with the inclusion of these chemical components. It also suggests, that influence of Ca-rich emissions such as concrete dust and fly ash from municipal waste combustion (viitteet), and Cu-enriched traffic emissions are underestimated in the current results. The combination of Cu, Zn, and Mg suggest the influence of traffic-related emissions, but Zn and K can be seen as indicator for biomass combustion. The high effect of Ca could be linked with PC3, soil dust, but it can be related to fly ash as well.

3.5.2. Oxidative stress

In the mixed model analysis of oxidative stress, exposure dose showed no significant effect in the model ($p = 0.091$), but incorporating it improved the model's fit to the data. This is an understandable result in light of the highly dissimilar responses observed in section 3.4.2. Time of day displayed a significant effect ($p = 1.4*10^{-5}$), indicating a substantial variation in oxidative stress due to time of day, which in this analysis applies to all PM size fractions pooled together. The principal components of PC1 ($p = 0.009$), PC2 ($p = 0.326$), and PC4 ($p = 0.399$), i.e. emissions from coal combustion and industry, traffic and oil/fuel combustion, and biomass combustion displayed interaction effects with exposure dose. These results suggest that the chemical components associated with coal combustion and industrial emissions explain a significant portion of the variation in the oxidative stress response, and their effect is dose-dependent.

PC1 had the greatest influence on the oxidative stress response when comparing the parameter estimates and displayed that at the dose of 50 µg/ml PC1 substantially increased the oxidative stress response (parameter estimate 32.75 % increased oxidative stress, 95% CI: 13.37, 52.12). With increasing doses, however, the response was greatly reduced: for 100 µg/ml dose the estimate was 11.24 % increased oxidative stress (95% CI: 1.99, 20.49), and ultimately for 200 µg/ml dose it fell to 2.05 % increased oxidative stress (95% CI: -2.56, 6.65) compared to control. This pattern is highly similar to that seen for daytime $PM_{0.2}$ from pre-intervention and post-intervention campaigns, which displayed rather high oxidative stress responses for the smallest dose and descending response levels for the higher doses. This effect by PC1 corresponds to its high factor value in $PM_{0.2}$ discussed in section 3.3.

While the effects of PC2 and PC4 on the oxidative stress response were not significant, their incorporation into the model improved the model fit. In contrast, PC3 ($p = 0.041$), i.e. soil dust, showed a significant interaction effect with time of day instead of dose, suggesting that the chemical components from this source showed no dose-dependent effects on oxidative stress, but their influence was different between day and nighttime. Time of day, by itself, had a large effect on the

oxidative stress elicited by PM, with daytime PM causing, in general, 13.1 % (95% CI: 7.6, 18.6) higher oxidative stress compared to night. Interestingly, the interaction term of PC3 and time of day produced modest increases for oxidative stress response compared to control, 6.23 %s (95% CI: 1.32, 11.15) for night and 4.30 % (95 % CI: -2.52, 11.12) for daytime samples. The difference between the effects of PC3 day and night was rather negligible, but together these results suggest that soil dust was associated with a slight increase of oxidative stress. Soil dust contains a wide array of transition metals, which have been associated with elevated oxidative stress levels in previous studies (Viitteet). This could also explain the high oxidative stress responses for $PM_{10-2.5}$, which typically contains a significant amount of soil dust particles, but due to its low contribution in other size fractions the estimate obtained from the combined dataset remains low. This is in agreement with the high factor value for PC3 in $PM_{10-2.5}$ discussed in section 3.3.

Changes in the BIC value for the truncated models with each PC removed separately confirmed that PC1 (coal combustion and industrial emissions) had the greatest effect on the oxidative stress response (BIC change of 4.9 %), followed by PC4 (biomass combustion, BIC change 3.4 %) and PC2 (traffic and fuel/oil combustion, 3.2 %). The smallest influence was observed for PC3 (soil dust, 2.8 %). These results suggest that while the effect for PC3 was significant and those for PC2 and PC4 were not, PC2 and PC4 explained more of the variation in the oxidative stress response. This highlights the problem of a combined dataset of different PM size fractions with distinct chemical compositions and toxicological effects, which could confound and mask the effects of different chemical components and emission sources in a pooled analysis. Alas, the sample size in the current study disallows size fraction-specific analyses.

A similar mixed model analysis was also performed on a select set of metals (Al, As, Fe, Mn, Na, Zn) to assess their contribution to oxidative stress. Other metals and PAHs were excluded from the analysis due to their observed collinearity. Thus, the selection of this set of metals was based purely on statistical grounds and does not indicate that these metals are the most important for causing oxidative stress in the current exposure system. Nevertheless, when comparing changes in the BIC values of the models one at a time, Al, Mn and As exhibited the greatest effects by a considerable margin (change in BIC values 9.6, 8.0, and 7.0 %, respectively). Next were Fe and Zn (3.9 and 3.7 %), while Na explained the smallest amount of variation in the model (BIC value change 2.3 %). Since the analysis does not separate the PM size ranges, the interpretation of these results is somewhat ambiguous. Still, Al, Mn, and Fe in larger particles are associated with crustal sources, whereas in smaller particles As, Mn, Fe, and Zn suggest the influence of coal and industrial combustion processes. Zn and Na demonstrate the role of biomass combustion, although they can be associated with industrial emissions as well. Additionally, Fe and Zn are linked with traffic emissions (viitteet näihin). Overall, these results support those observed for the PCs, emphasizing the influence of coal and industrial combustion processes.

4. Conclusions

In general, the cytotoxicity and oxidative stress caused by PM were reduced due to the air quality intervention for all size fractions except $PM_{0.2}$. The seasonal variations of emission sources, air mass trajectories, and weather conditions confound the causes of toxicological variation seen for $PM_{0.2}$. However, $PM_{0.2}$ mass concentration was clearly diminished during the intervention at an urban background location, but this effect was more modest in downtown Nanjing. Coal and industrial combustion processes were the primary emission sources of $PM_{0.2}$ in the current study;

yet, their contribution to the PM composition showed no changes due to the air quality intervention. This is an interesting and alarming finding since $PM_{0.2}$ is regarded as the most harmful PM size fraction and is an issue worth further research.

The air quality intervention was successful in reducing the mass concentration of airborne PM_{10} by over 50 %; conversely, $PM_{2.5}$ was practically enriched since the emission controls reduced $PM_{10-2.5}$ mass concentration the most. Contributions of soil dust, including construction dust, and biomass combustion emissions on PM_{10} composition were decreased during the intervention period. In contrast, the influence of traffic was dramatically increased. Additionally, the atmospheric processes emphasized the effects of local emissions during the intervention campaign.

Coal and industrial combustion emissions affected the cytotoxicity clearly in a dose-dependent manner, whereas biomass combustion had the greatest individual influence on it without displaying dose-dependence. Coal and industrial combustion processes also showed a great influence on the oxidative stress response. The eminent role of traffic emissions during the intervention and the observed lower cytotoxicity of intervention samples are in an interesting conflict. This finding contradicts the generally accepted role of traffic emissions being among the main culprits of PM-associated adverse health effects. However, the effect of traffic emissions on cytotoxicity and oxidative stress may be underestimated in the currently employed statistical model due to limitations of the dataset.

Acknowledgements

The authors wish to thank Ms. Hanne Vainikainen, Ms. Maija Sainio, and Ms. Sonja Pennanen for their efforts and technical expertise in the present study.

Funding

This work was supported by the Academy of Finland (grants 278269, 278331, 287982, 294081, and 304459) and the University of Eastern Finland Doctoral School. The funding sources were not involved in the design, execution, or reporting of the current study.

References

1. Abbas I., Badran G., Verdin A., Ledoux F., Roumié M., Courcot D., Garçon G. 2018. Polycyclic aromatic hydrocarbon derivatives in airborne particulate matter: Sources, analysis and toxicity. Environmental Chemistry Letters 16 2: 439-475. DOI:10.1007/s10311-017-0697-0.
2. Burnett R., Chen H., Szyszkowicz M., Fann N., Hubbell B., Pope C.A. . . . Spadaro J.V. 2018. Global estimates of mortality associated with long-term exposure to outdoor fine particulate matter. Proceedings of the National Academy of Sciences 115 38: 9592-9597. DOI:10.1073/pnas.1803222115.
3. Cohen A.J., Brauer M., Burnett R., Anderson H.R., Frostad J., Estep K. . . . Forouzanfar M.H. 2017. Estimates and 25-year trends of the global burden of disease attributable to ambient air pollution: An analysis of data from the global burden of diseases study 2015. The Lancet 389 10082: 1907-1918. DOI:10.1016/S0140-6736(17)30505-6.
4. Ding J., van der A, R. J., Mijling B., Levelt P.F., Hao N. 2015. NOx emission estimates during the 2014 youth olympic games in nanjing. Atmospheric Chemistry and Physics 15 16: 9399-9412. DOI:10.5194/acp-15-9399-2015.

5. Forouzanfar M.H., Alexander L., Anderson H.R., Bachman V.F., Biryukov S., Brauer M. . . . Murray C.J. 2015. Global, regional, and national comparative risk assessment of 79 behavioural, environmental and occupational, and metabolic risks or clusters of risks in 188 countries, 1990–2013: A systematic analysis for the global burden of disease study 2013. The Lancet 386 10010: 2287-2323. DOI://doi.org/10.1016/S0140-6736(15)00128-2.
6. Fu F., Tian B., Lin G., Chen Y., Zhang J. 2010. Chemical characterization and source identification of polycyclic aromatic hydrocarbons in aerosols originating from different sources. Journal of the Air & Waste Management Association 60 11: 1309-1314. DOI:10.3155/1047-3289.60.11.1309.
7. Gakidou E., Afshin A., Abajobir A.A., Abate K.H., Abbafati C., Abbas K.M. . . . Murray C.J.L. 2017. Global, regional, and national comparative risk assessment of 84 behavioural, environmental and occupational, and metabolic risks or clusters of risks, 1990-2016: A systematic analysis for the global burden of disease study 2016. The Lancet 390 10100: 1345-1422. DOI:10.1016/S0140-6736(17)32366-8.
8. Ghio A.J., Kummarapurugu S.T., Tong H., Soukup J.M., Dailey L.A., Boykin E. . . . Reynolds R.L. 2014. Biological effects of desert dust in respiratory epithelial cells and a murine model. Inhalation Toxicology 26 5: 299-309. DOI:10.3109/08958378.2014.888109.
9. Hu Q., Li X., Lin A., Qi W., Li X., Yang X.J. 2018. Total emission control policy in china. Environmental Development 25 126-129. DOI://doi.org/10.1016/j.envdev.2017.11.002.
10. Jalava P.I., Wang Q., Kuuspalo K., Ruusunen J., Hao L., Fang D. . . . Hirvonen M.-. 2015. Day and night variation in chemical composition and toxicological responses of size segregated urban air PM samples in a high air pollution situation. Atmospheric Environment 120 427-437. DOI://doi.org/10.1016/j.atmosenv.2015.08.089.
11. Jalava P.I., Salonen R.O., Hälinen A.I., Penttinen P., Pennanen A.S., Sillanpää M. . . . Hirvonen M.-.R. 2006. In vitro inflammatory and cytotoxic effects of size-segregated particulate samples collected during long-range transport of wildfire smoke to helsinki. Toxicology and Applied Pharmacology 215 3: 341-353. DOI://dx.doi.org/10.1016/j.taap.2006.03.007.
12. Jin L., Xie J., Wong C.K.C., Chan S.K.Y., Abbaszade G., Schnelle-Kreis J. . . . Li X. 2019. Contributions of city-specific fine particulate matter (PM2.5) to differential in vitro oxidative stress and toxicity implications between beijing and guangzhou of china. Environmental Science & Technology 53 5: 2881-2891. DOI:10.1021/acs.est.9b00449.
13. Kang M., Yang F., Ren H., Zhao W., Zhao Y., Li L. . . . Fu P. 2017. Influence of continental organic aerosols to the marine atmosphere over the east china sea: Insights from lipids, PAHs and phthalates. Science of the Total Environment 607-608 339-350. DOI://doi.org/10.1016/j.scitotenv.2017.06.214
14. Kasurinen S., Happo M.S., Rönkkö T.J., Orasche J., Jokiniemi J., Kortelainen M. . . . Jalava P.I. 2018. Differences between co-cultures and monocultures in testing the toxicity of particulate matter derived from log wood and pellet combustion. PLoS One 13 2: e0192453. DOI://dx.doi.org/10.1371/journal.pone.0192453.
15. Kasurinen S., Jalava P.I., Happo M.S., Sippula O., Uski O., Koponen H. . . . Hirvonen M. 2017. Particulate emissions from the combustion of birch, beech, and spruce logs cause different cytotoxic responses in A549 cells. Environmental Toxicology 32 5: 1487-1499. DOI:10.1002/tox.22369.
16. Li C.K.,Kamens R.M. 1993. The use of polycyclic aromatic hydrocarbons as source signatures in receptor modeling. Atmospheric Environment. Part A. General Topics 27 4: 523-532. DOI://doi.org/10.1016/0960-1686(93)90209-H
17. Li M., Shi S., Wang T.-. 2012. Identification and distribution of chrysene, methylchrysenes and their isomers in crude oils and rock extracts. Organic Geochemistry 52 55-66. DOI://doi.org/10.1016/j.orggeochem.2012.08.011
18. Li S., Li H., Luo J., Li H., Qian X., Liu M. . . . Ma L.Q. 2016. Influence of pollution control on lead inhalation bioaccessibility in PM2.5: A case study of 2014 youth olympic games in nanjing. Environment International 94 69-75. DOI://doi.org/10.1016/j.envint.2016.05.010

19. Mazidi M.,Speakman J.R. 2017. Ambient particulate air pollution (PM2.5) is associated with the ratio of type 2 diabetes to obesity. Scientific Reports 7 1: 9144. DOI:10.1038/s41598-017-08287-1.
20. Miettinen M., Leskinen A., Abbaszade G., Orasche J., Sainio M., Mikkonen S. . . . Sippula O. 2018. PM2.5 concentration and composition in the urban air of nanjing, china: Effects of emission control measures applied during the 2014 youth olympic games. Science of the Total Environment 362 1-18. DOI:10.1016/j.scitotenv.2018.10.191.
21. Ohura T., Amagai T., Fusaya M., Matsushita H. 2004. Polycyclic aromatic hydrocarbons in indoor and outdoor environments and factors affecting their concentrations. Environmental Science & Technology 38 1: 77-83. DOI:10.1021/es030512o.
22. Oliveira C., Martins N., Tavares J., Pio C., Cerqueira M., Matos M. . . . Camões F. 2011. Size distribution of polycyclic aromatic hydrocarbons in a roadway tunnel in lisbon, portugal. Chemosphere 83 11: 1588-1596. DOI://doi.org/10.1016/j.chemosphere.2011.01.011
23. Park M., Joo H.S., Lee K., Jang M., Kim S.D., Kim I. . . . Park K. 2018. Differential toxicities of fine particulate matters from various sources. Scientific Reports 8 1: 17007. DOI:10.1038/s41598-018-35398-0.
24. Pearson J.F., Bachireddy C., Shyamprasad S., Goldfine A.B., Brownstein J.S. 2010. Association between fine particulate matter and diabetes prevalence in the U.S. Diabetes Care 33 10: 2196-2201. DOI:10.2337/dc10-0698.
25. Portnov B.A., Reiser B., Karkabi K., Cohen-Kastel O., Dubnov J. 2012. High prevalence of childhood asthma in northern israel is linked to air pollution by particulate matter: Evidence from GIS analysis and bayesian model averaging. International Journal of Environmental Health Research 22 3: 249-269.
26. Qi L., Zhang Y., Ma Y., Chen M., Ge X., Ma Y. . . . Li S. 2016. Source identification of trace elements in the atmosphere during the second asian youth games in nanjing, china: Influence of control measures on air quality. Atmospheric Pollution Research 7 3: 547-556. DOI://dx.doi.org/10.1016/j.apr.2016.01.003.
27. Rolph G., Stein A., Stunder B. 2017. Real-time environmental applications and display sYstem: READY. Environmental Modelling & Software 95 210-228. DOI://doi.org/10.1016/j.envsoft.2017.06.025
28. Rönkkö T.J., Jalava P.I., Happo M.S., Kasurinen S., Sippula O., Leskinen A. . . . Hirvonen M. 2018. Emissions and atmospheric processes influence the chemical composition and toxicological properties of urban air particulate matter in nanjing, china. Science of the Total Environment 639 1290-1310. DOI://doi.org/10.1016/j.scitotenv.2018.05.260.
29. Sillanpää M., Hillamo R., Mäkelä T., Pennanen A.S., Salonen R.O. 2003. Field and laboratory tests of a high volume cascade impactor. Journal of Aerosol Science 34 4: 485-500. DOI://doi.org/10.1016/S0021-8502(02)00214-8.
30. Sippula O., Rintala H., Happo M., Jalava P., Kuuspalo K., Virén A. . . . Hirvonen M.-.R. 2013. Characterization of chemical and microbial species from size-segregated indoor and outdoor particulate samples. Aerosol Air Qual Res 13 1212-1230.
31. Song C., He J., Wu L., Jin T., Chen X., Li R. . . . Mao H. 2017. Health burden attributable to ambient PM2.5 in china. Environmental Pollution 223 575-586. DOI://doi.org/10.1016/j.envpol.2017.01.060.
32. Stein A.F., Draxler R.R., Rolph G.D., Stunder B.J.B., Cohen M.D., Ngan F. 2015. NOAA's HYSPLIT atmospheric transport and dispersion modeling system. Bulletin of the American Meteorological Society 96 12: 2059-2077. DOI:10.1175/BAMS-D-14-00110.1.
33. Tapanainen M., Jalava P.I., Mäki-Paakkanen J., Hakulinen P., Lamberg H., Ruusunen J. . . . Hirvonen M. 2012. Efficiency of log wood combustion affects the toxicological and chemical properties of emission particles. Inhalation Toxicology 24 6: 343-355. DOI:10.3109/08958378.2012.671858.

34. Velali E., Papachristou E., Pantazaki A., Besis A., Samara C., Labrianidis C., Lialiaris T. 2018. In vitro cellular toxicity induced by extractable organic fractions of particles exhausted from urban combustion sources - role of PAHs. Environmental Pollution 243 1166-1176. DOI://doi.org/10.1016/j.envpol.2018.09.075
35. Wang G., Kawamura K., Xie M., Hu S., Gao S., Cao J. . . . Wang Z. 2009. Size-distributions of n-alkanes, PAHs and hopanes and their sources in the urban, mountain and marine atmospheres over east asia. Atmospheric Chemistry and Physics 9 22: 8869-8882. DOI:10.5194/acp-9-8869-2009.
36. Wang H., An J., Cheng M., Shen L., Zhu B., Li Y. . . . Xia L. 2016. One year online measurements of water-soluble ions at the industrially polluted town of nanjing, china: Sources, seasonal and diurnal variations. Chemosphere 148 Supplement C: 526-536. DOI://doi.org/10.1016/j.chemosphere.2016.01.066.
37. Wang T., Xia Z., Wu M., Zhang Q., Sun S., Yin J. . . . Yang H. 2017. Pollution characteristics, sources and lung cancer risk of atmospheric polycyclic aromatic hydrocarbons in a new urban district of nanjing, china. Journal of Environmental Sciences 55 Supplement C: 118-128. DOI://doi.org/10.1016/j.jes.2016.06.025.
38. World Health Organization, International Programme on Chemical Safety. 1998. Selected Non-Heterocyclic Polycyclic Aromatic Hydrocarbons. World Health Organization. Geneva.
39. Yang L., Cheng S., Wang X., Nie W., Xu P., Gao X. . . . Wang W. 2013. Source identification and health impact of PM2.5 in a heavily polluted urban atmosphere in china. Atmospheric Environment 75 265-269. DOI://doi.org/10.1016/j.atmosenv.2013.04.058.
40. Yu J.Z., Huang X.H.H., Ho S.S.H., Bian Q. 2011. Nonpolar organic compounds in fine particles: Quantification by thermal desorption–GC/MS and evidence for their significant oxidation in ambient aerosols in hong kong. Analytical and Bioanalytical Chemistry 401 10: 3125-3139. DOI:10.1007/s00216-011-5458-5.
41. Yuan F., Gao J., Wang L., Cai Y. 2017. Co-location of manufacturing and producer services in nanjing, china. Cities 63 Supplement C: 81-91. DOI://doi.org/10.1016/j.cities.2016.12.021.
42. Yunker M.B., Macdonald R.W., Vingarzan R., Mitchell R.H., Goyette D., Sylvestre S. 2002. PAHs in the fraser river basin: A critical appraisal of PAH ratios as indicators of PAH source and composition. Organic Geochemistry 33 4: 489-515. DOI://doi.org/10.1016/S0146-6380(02)00002-5.
43. Zhang F., Chen Y., Tian C., Wang X., Huang G., Fang Y., Zong Z. 2014. Identification and quantification of shipping emissions in bohai rim, china. Science of the Total Environment 497-498 570-577. DOI://doi.org/10.1016/j.scitotenv.2014.08.016
44. Zhang Y., Schauer J.J., Zhang Y., Zeng L., Wei Y., Liu Y., Shao M. 2008. Characteristics of particulate carbon emissions from real-world chinese coal combustion. Environmental Science & Technology 42 14: 5068-5073. DOI:2048/10.1021/es7022576.
45. Zhao H., Zheng Y., Li T. 2017. Air quality and control measures evaluation during the 2014 youth olympic games in nanjing and its surrounding cities. Atmosphere 8 6:DOI:10.3390/atmos8060100
46. Zhou D., Li B., Huang X., Virkkula A., Wu H., Zhao Q. . . . Ding A. 2017. The impacts of emission control and regional transport on PM2.5 ions and carbon components in nanjing during the 2014 nanjing youth olympic games. Aerosol and Air Quality Research 17 3: 730-740. DOI:10.4209/aaqr.2016.03.0131.
47. Zhou S., Yuan Q., Li W., Lu Y., Zhang Y., Wang W. 2014. Trace metals in atmospheric fine particles in one industrial urban city: Spatial variations, sources, and health implications. Journal of Environmental Sciences 26 1: 205-213. DOI://doi.org/10.1016/S1001-0742(13)60399-X
48. Zou B., You J., Lin Y., Duan X., Zhao X., Fang X. . . . Li S. 2019. Air pollution intervention and life-saving effect in china. Environment International 125 529-541. DOI://doi.org/10.1016/j.envint.2018.10.045